A FINITE ELEMENT STUDY OF THE EFFECTIVE WIDTH OF SIMPLE AND CONTINUOUS T-BEAMS

RAMAPADA KAR

A DISSERTATION

in the

Faculty of Engineering

Presented in partial fulfilment of the requirements for
the Degree of Master of Engineering at
Sir George Williams University
Montreal, Canada

September 1973

ABSTRACT

ABSTRACT

A three-dimensional finite element study on the effective width of simple and continuous T-beams is presented. The 20-node isoparametric solid elements are used for the analysis.

Classical approach of investigating these beams has also been reviewed.

Both methods are used to determine the distribution of stresses in the flange of a number of T-beams. The results when compared, show close agreement.

The effective widths of the beams determined by the classical approach and the finite element technique are then compared with those obtained by using the CSA Standard A23.3-1970, Canadian Code For the Design of Plain or Reinforced Concrete Structures. The results of comparison are found to be within the acceptable limits of practical design.

ACKNOWLEDGEMENTS

ACKNOWLEDGEMENTS

The work presented in this dissertation was carried out under the direct supervision of Dr. M.S. Troitsky, Professor of Engineering, to whom the author wishes to express his deepest gratitude for his guidance and encouragement.

The facilities provided by the Computer Centre of Sir George Williams University are gratefully acknowledged.

Thanks are also due to Miss M. Stredder for typing this manuscript.

CONTENTS

TABLE OF CONTENTS

FIGURES

LIST OF FIGURES

TABLES

LIST OF TABLES

NOTATIONS

NOTATIONS

The following list defines the principal symbols used in this dissertation. For convenience of reference, these are summarized for each chapter individually. Other symbols are defined in the text.

Rectangular matrices are indicated by brackets [ ] and column vectors by braces { }.

CHAPTER 2

b	half the clear distance between ribs
b_e	effective overhanging width of flange
b_{es}	effective width of flange for symmetrically loaded ribs
b_{esn}	effective width of flange for symmetrically loaded ribs for the n-th harmonic
b_o	width of rib
d	thickness of flange
d_o	overall depth of T-beam
F	Airy's stress function
F_a	antisymmetric part of the Airy's stress function F
F_{ns}	symmetric part of the Airy's stress function F for the n-th harmonic
F_s	symmetric part of the Airy's stress function F
L	span length of T-beam
p	intensity of load

CHAPTER 2 (continued)

u, v	displacements in the x and y directions respectively
Z_b	section modulus for the bottom of rib
Z_{be}	section modulus of T-beam with actual flange width b replaced by b_{es}
Z_{kn}	section modulus for the n-th harmonic referred to line K
Z_o	section modulus of the rib only
Z_t	section modulus for the top fibre
σ_x, σ_y	stresses in the x and y directions respectively
σ_{xb}	σ_x at $y = b$
σ_{xbn}	σ_{xb} for the n-th harmonic
$\bar{\sigma}_{xbn}$	maximum σ_{xbn}
σ_{oxb}	σ_x at $y = b$ in the flange plate at midspan of beam
α_n	$n\pi/L$
β	$2b/b_o$
γ	$2b/L$
δ	d/d_o
λ_n	b_{esn}/b

CHAPTER 3

[B]	transformation matrix relating strains and displacements
[D]	constitutive (stress-strain) matrix
{F}	vector of nodal forces
[J]	Jacobian matrix
[k]	element stiffness matrix
[K]	overall stiffness matrix
[N]	matrix of shape functions
N_i	shape function for node i
{p}	vector of load intensities
{q}	vector of generalized displacements
{Q}	vector of the work-equivalent nodal forces
u,v,w	displacements in the x,y,z-directions respectively
x,y,z	Cartesian co-ordinates
α,β,γ	local coordinates
$\{\delta\}$	vector of global displacements
$\{\varepsilon\}$	vector of strains
$\{\sigma\}$	vector of stresses

CHAPTER 1

INTRODUCTION

CHAPTER 1

INTRODUCTION

In reinforced concrete design, the T-beam constitutes a very common and effective load-carrying element. The flange and the rib of a T-beam are monolithically connected, and the classical analysis of the flange rests on separating it from the rib and then determining the stresses by using the principles of continuum mechanics.

The Building Codes provide simplified rules for a practical design. The first step lies in establishing what is known as the effective width of a T-beam.

The elementary theory of bending of beams predicts a linear distribution of the stress across any section. The assumption that the plane section remains plane after bending is not, however, true for T-beams with wide flanges. The flange is loaded in its plane along its line of connection with the web. Because of shear strain in the flange, its longitudinal stresses are distributed non-uniformly throughout its width. Fig. 1.1 shows the stress distribution in the flange. To simplify the calculation of the maximum stress and deformation caused by the bending of the beam, the actual width of the flange is replaced by an imaginary width, b_e, referred to as the effective width. The longitudinal stress in the flange is assumed to be constant over the width b_e

and equal to the maximum stress in the web at the line of contact, as indicated in Fig. 1.2.

Classical works on effective width by von Karman [1] and Chwalla [2] have been the basis of many other studies. Most of these theoretical investigations assume that the flange plate is very thin, compared to the overall depth of the beam. For a thin plate shear resistance is more dominant than its bending action. Consequently, only the in-plane action of the flange is taken into consideration. The bending action of the flange in the longitudinal direction is neglected. This assumption requires that all loads are applied in a vertical plane through the longitudinal axis of the web. It is also implied that the flange plate is connected to the web, not across the thickness, but along a line of contact placed at the middle surface of the plate, as shown in Fig. 1.2.

Koepcke and Denecke [3] have studied both the simple span and continuous beams and provide useful tables for easier computation of the compressive force on the flange plate, the maximum stress and the effective width. Again, only the membrane action is considered. Marguerre's [4] investigation includes both in-plane and bending action of the plate. Brendel [5] has made a comparative study of the effective width formulas in the reinforced concrete Codes of various countries. Several other authors [6,7,8,9] provide useful information on the subject.

Abdel-Sayed [10] concludes that the ratio of the cross-sectional area of the web to the cross-sectional area of the plate has a significant effect on the effective flange width. Due to the bending of the beam as a whole, the flange plate also undergoes bending and the influence of such bending is even more significant if the ratio of the flange thickness to the overall beam depth is comparatively large. In reinforced and prestressed concrete construction a ratio of 1/4 is not uncommon.

Literature on the study of effective width of continuous beams is scarce. Usually, the length between the two points of contraflexure in a span is treated as a simple span. The behaviour of the flange over a continuous support is not well documented. In certain practical applications, it is useful to know the distribution of tensile stress along the width of the flange in the negative moment zone.

The objectives of this dissertation are threefold. The first is to outline the classical approach for the analysis of simply supported T-beams. The second is to apply the finite element technique to investigate the flange stresses for both simple and continuous span beams. A three-dimensional isoparametric solid element has been chosen for this purpose. The third is to compare the results obtained by both methods.

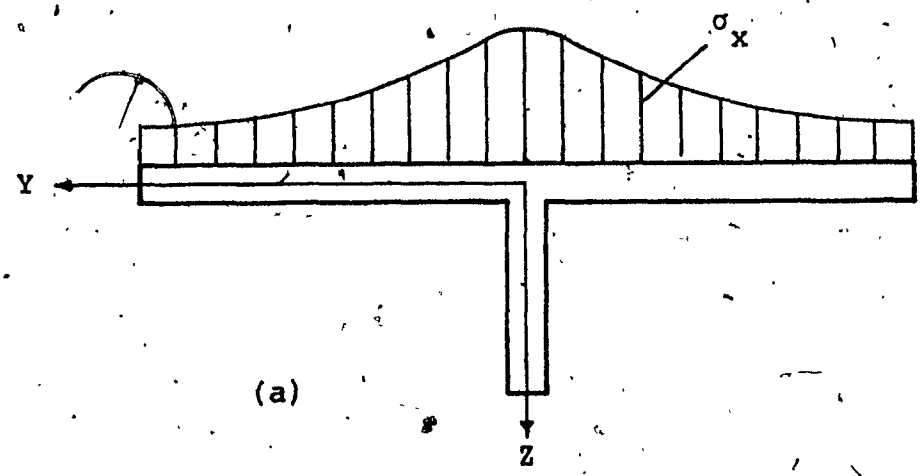

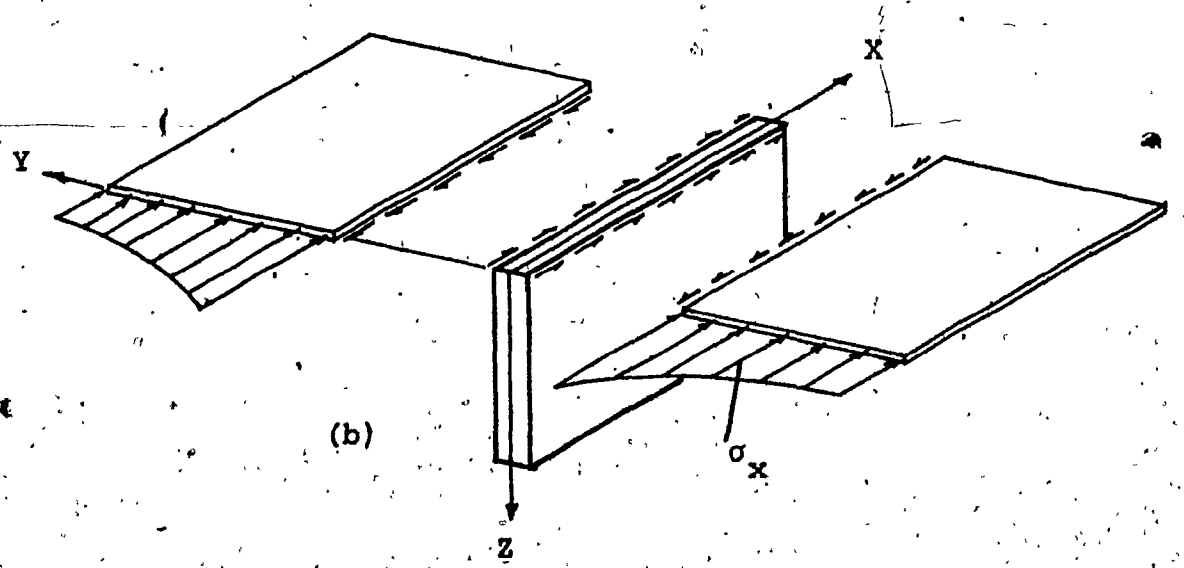

FIG. 1.1 Longitudinal Stress Distribution in the Flange of T-Beam

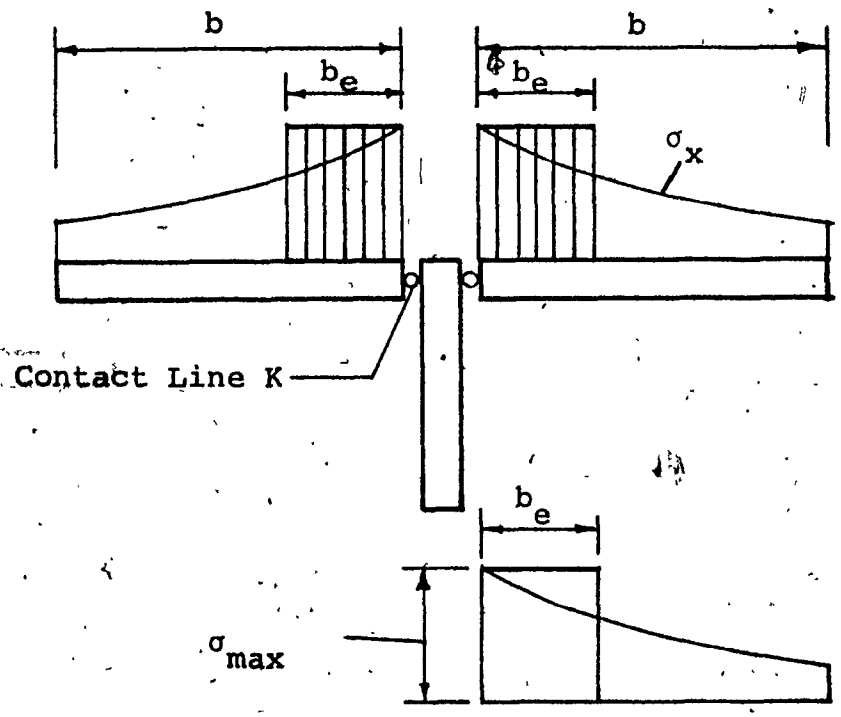

FIG. 1.2 Effective Width of T-Beam

CHAPTER 2

CLASSICAL THEORY OF T-BEAMS

CHAPTER 2

CLASSICAL THEORY OF T-BEAMS

2.1 DERIVATION OF EFFECTIVE WIDTH

Consider a single span beam-system consisting of a series of T-beams. Loads of equal intensity are applied in the vertical planes passing through the longitudinal axis of the ribs. Due to symmetry, the flange plate between two consecutive beams can be separated out for the purpose of analysis, as shown in Fig. 2.1. It will be assumed that the depth of the beam is small compared to the span L and that straight line distribution of bending stress is valid for the ribs. For convenience of analysis, the flange plate is assumed to be connected to the rib along a line of contact K placed at the middle plane of the plate, as indicated in Fig. 2.1 (c). Shear stresses at the contact line force the rib and the plate to undergo equal strain, satisfying the compatibility conditions. The plate itself, therefore, is in a state of two-dimensional stress, as shown in Fig. 2.1 (d).

From the theory of elasticity, the equations of equilibrium are

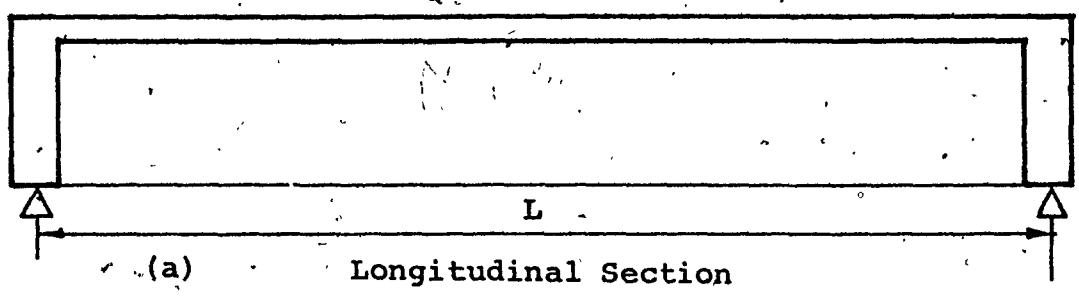

(a) Longitudinal Section

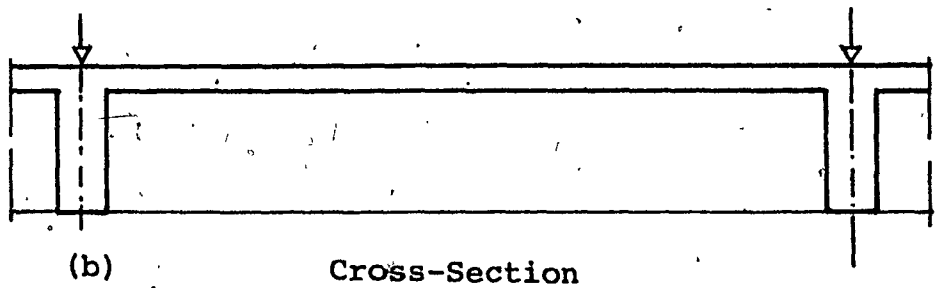

(b) Cross-Section

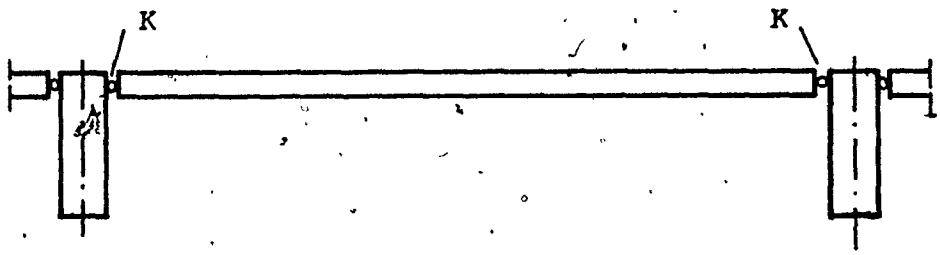

(c) Idealization

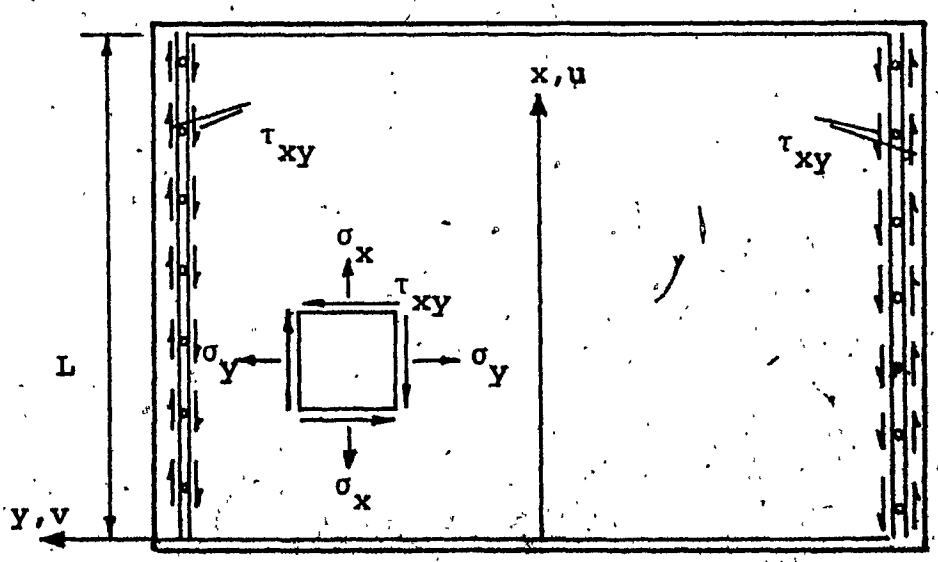

(d) Plan of Flange Plate

FIG. 2.1 Flange Plate Between Ribs

$$\frac{\partial \sigma_x}{\partial x} + \frac{\partial \tau_{xy}}{\partial y} = 0$$

$$\frac{\partial \sigma_y}{\partial y} + \frac{\partial \tau_{xy}}{\partial x} = 0 \qquad (2.1)$$

$$\tau_{xy} = \tau_{yx}$$

The strain-displacement relations are

$$\varepsilon_x = \frac{\partial u}{\partial x} \; ; \quad \varepsilon_y = \frac{\partial v}{\partial y} \; ; \quad \gamma_{xy} = \frac{\partial u}{\partial y} + \frac{\partial v}{\partial x} \qquad (2.2)$$

$$\varepsilon_x = \frac{1}{E}(\sigma_x - \nu\sigma_y) \; ; \quad \varepsilon_y = \frac{1}{E}(\sigma_y - \nu\sigma_x) \; ; \quad \gamma_{xy} = \frac{2(1+\nu)}{E}\tau_{xy} \qquad (2.3)$$

From Eqs. (2.2), the compatibility Eq. (2.4) is obtained.

$$\frac{\partial^2 \varepsilon_x}{\partial y^2} + \frac{\partial^2 \varepsilon_y}{\partial x^2} - \frac{\partial^2 \gamma_{xy}}{\partial x \partial y} = 0 \qquad (2.4)$$

Substitution of Eq. (2.3) into (2.4) yields

$$\frac{\partial^2 \sigma_y}{\partial x^2} - 2\frac{\partial^2 \tau_{xy}}{\partial x \partial y} + \frac{\partial^2 \sigma_x}{\partial y^2} - \nu\left(\frac{\partial^2 \sigma_x}{\partial x^2} + 2\frac{\partial^2 \tau_{xy}}{\partial x \partial y} + \frac{\partial^2 \sigma_y}{\partial y^2}\right) = 0 \qquad (2.5)$$

The equilibrium Eqs. (2.1) will be fulfilled by expressing σ_x, σ_y, τ_{xy} by means of Airy's stress function F,

$$\sigma_x = \frac{\partial^2 F}{\partial y^2} \; ; \quad \sigma_y = \frac{\partial^2 F}{\partial x^2} \; ; \quad \tau_{xy} = -\frac{\partial^2 F}{\partial x \partial y} \qquad (2.6)$$

If Eqs. (2.6) are substituted into (2.5), the expression within the parentheses vanishes, giving the governing differential equation for the flange plate

$$\frac{\partial^4 F}{\partial x^4} + 2\,\frac{\partial^4 F}{\partial x^2 \partial y^2} + \frac{\partial^4 F}{\partial y^4} = 0 \qquad (2.7)$$

The stress function that satisfies this equation is

$$F = \sum_{n=1,2,3\ldots}^{\infty} (A_n \cosh\alpha_n y + B_n y \sinh\alpha_n y + C_n \sinh\alpha_n y + D_n y \cosh\alpha_n y) \cdot$$

$$\cdot \sin\alpha_n x \quad \text{where} \quad \alpha = \frac{n\pi}{L} \qquad (2.8)$$

Referred to the y-axis, F can be broken into a symmetrical part F_s and an antisymmetrical part F_a as follows:

$$F_s = \sum_n (A_n \cosh\alpha_n y + B_n y \sinh\alpha_n y) \sin\alpha_n x$$

$$F_a = \sum_n (C_n \sinh\alpha_n y + D_n y \cosh\alpha_n y) \sin\alpha_n x \qquad (2.9)$$

Replacing the bracketed terms in (2.8) and (2.9) by f_n, f_{ns} and f_{na}, respectively, one obtains

$$F = \sum_n f_n \sin\alpha_n x$$

$$F_s = \sum_n f_{ns} \sin\alpha_n x \qquad (2.10)$$

$$F_a = \sum_n f_{na} \sin\alpha_n x$$

Using Eq. (2.6), the stresses in the plate are

$$\sigma_x = \sum_n \frac{d^2 f_n}{dy^2} \sin\alpha_n x$$

$$\sigma_y = -\sum_n f_n \alpha^2{}_n \sin\alpha_n x \qquad (2.11)$$

$$\tau_{xy} = -\sum_n \frac{df_n}{dy} \alpha_n \cos\alpha_n x$$

If both the ribs are equally loaded, σ_x will be symmetric about the x-axis and its distribution will be as shown in Fig. 2.2.

Replacing the σ_x-diagram by an equivalent rectangle, the effective width is defined as

$$b_e \, \sigma_{xb} = \int_o^b \sigma_x \, dy \qquad (2.12)$$

It is evident that along the x-axis, the symmetry axis, the shear stress $\tau_{xy} = 0$.

Substitution of (2.11) into (2.12) yields

$$b_e \, \sigma_{xb} = \int_o^b \sigma_x \, dy = \int_o^b \sum \frac{d^2 f_n}{dy^2} \sin\alpha_n x \, dy$$

$$= \sum_n \frac{df_n}{dy} \Big|_o^b \sin\alpha_n x$$

$$= \sum_n \left[\left(\frac{df_n}{dy}\right)_{y=b} - \left(\frac{df_n}{dy}\right)_{y=o} \right] \sin\alpha_n x$$

Since $\sigma_{xb} = \sum_n \left(\frac{d^2 f_n}{dy^2}\right)_{y=b} \sin\alpha_n x$, it follows

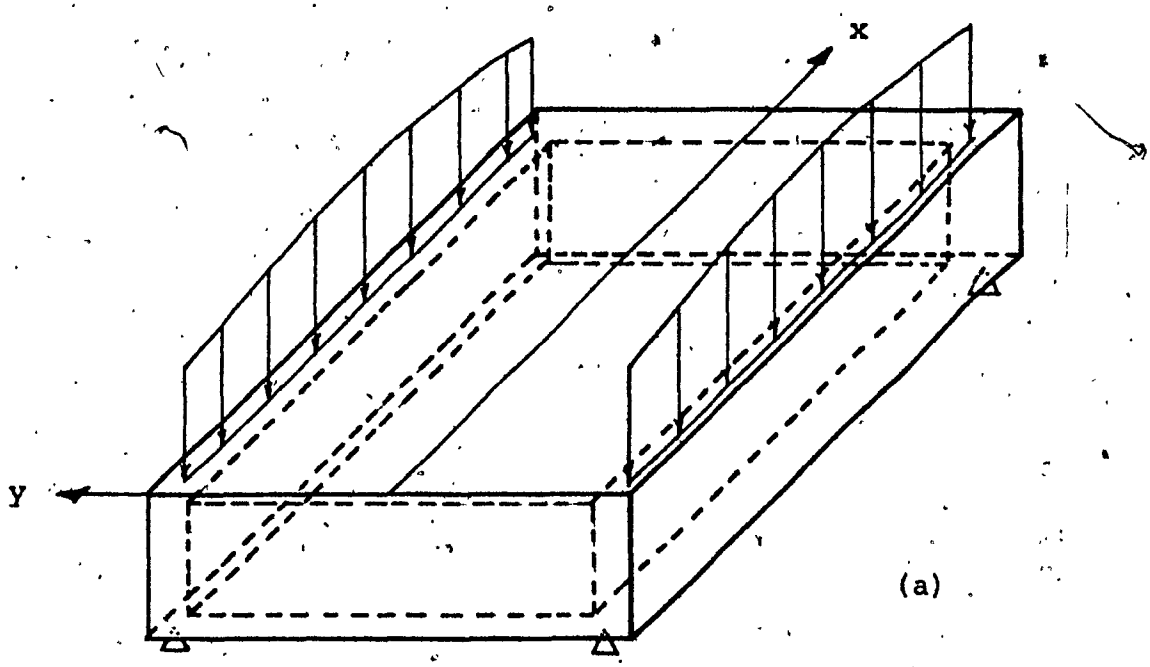

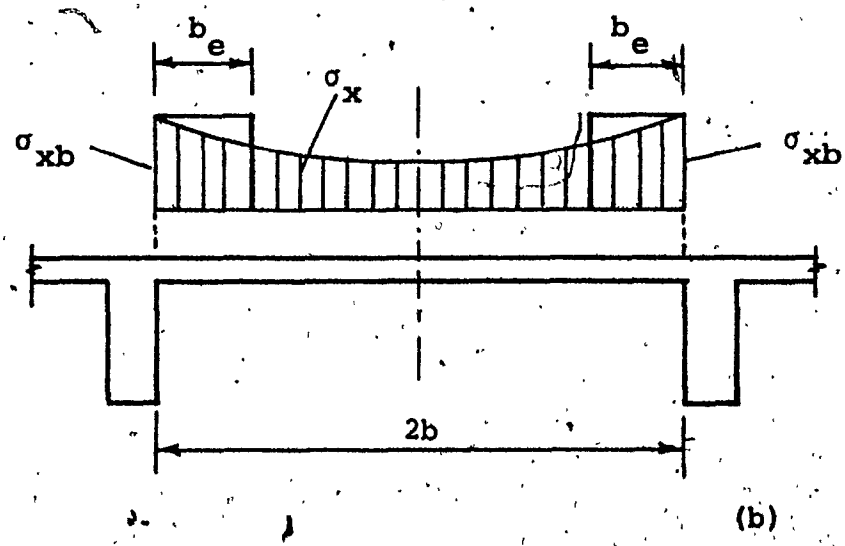

FIG. 2.2 Symmetrically Loaded Ribs

that

$$b_e = \frac{\sum_n \frac{df_n}{dy}\Big|_o^b \sin\alpha_n x}{\sum_n \left(\frac{d^2 f_n}{dy^2}\right)_{y=b} \sin\alpha_n x} \qquad (2.13)$$

For symmetrical cases, $\sum_n \left(\frac{df_{ns}}{dy}\right)_{y=o} = 0$. Hence

$$b_{es} = \frac{\sum_n \frac{df_{ns}}{dy})_{y=b} \sin\alpha_n x}{\sum_n \left(\frac{d^2 f_{ns}}{dy^2}\right)_{y=b} \sin\alpha_n x} \qquad (2.14)$$

This shows that along the span length L, effective width b_e is a function of x. Expression on the right-hand side of Eqn. (2.14) contains the unknown constants A_n and B_n. These constants are determined from the boundary conditions of the plate.

2.2 BOUNDARY CONDITIONS FOR THE FLANGE PLATE

It is usual practice to provide cross-beams at the end support of T-beams. In establishing the boundary conditions for the plate, it will be assumed that transverse beams, if any, are rigid in their own planes but offer no resistance in a direction perpendicular to them. In other words

$$v = 0$$
$$\sigma_x = 0 \tag{2.15}$$

Since the displacement v along the whole length of the end beam is zero, it also follows that

$$\frac{\partial v}{\partial y} = \varepsilon_y = \frac{1}{E}(\sigma_y - \nu\sigma_x) = 0$$

Substitution of (2.15) gives $\sigma_y = 0$. Hence the boundary conditions are at $x = o$ and $x = L$ are

$$\sigma_x = \frac{\partial^2 F}{\partial y^2} = 0$$
$$\sigma_y = \frac{\partial^2 F}{\partial x^2} = 0 \tag{2.16}$$

It will be noted that for $x = 0$ and $x = L$ these conditions are immediately satisfied for each term in the expression for F in Eqn. (2.8).

To establish the boundary conditions at the connection to the ribs, it is noted that due to vertical loading the flange plates on either side of the rib prevent any horizontal displacement of the contact line K. An additional requirement is that the longitudinal strain of the rib and the plate at line K is the same. However, it will be evident later that

this second condition does not explicitly enter the formulation. So for $y = \pm b$, $v = 0$. It follows then,

$$\frac{\partial v}{\partial x} = 0$$
$$\frac{\partial^2 v}{\partial x^2} = 0 \tag{2.17}$$

Using Eqns. (2.2), (2.3) and (2.6), and after proper differentiation the following two equations can be obtained

$$\frac{\partial^2 u}{\partial x \partial y} = \frac{1}{E}\left(\frac{\partial \sigma_x}{\partial y} - \nu \frac{\partial \sigma_y}{\partial y}\right) = \frac{1}{E}\left(\frac{\partial^3 F}{\partial y^3} - \nu \frac{\partial^3 F}{\partial x^2 \partial y}\right) \tag{2.18}$$

$$\frac{\partial^2 u}{\partial x \partial y} + \frac{\partial^2 v}{\partial x^2} = \frac{2(1+\nu)}{E} \frac{\partial \tau_{xy}}{\partial x} = -\frac{2(1+\nu)}{E} \frac{\partial^3 F}{\partial x^2 \partial y} \tag{2.19}$$

Subtracting (2.19) from (2.18)

$$-E \frac{\partial^2 v}{\partial x^2} = \frac{\partial^3 F}{\partial y^3} + (2+\nu) \frac{\partial^3 F}{\partial x^2 \partial y} \tag{2.20}$$

Using Eqns. (2.17) and (2.20) an equivalent boundary condition for $v = 0$ is

$$\frac{\partial^3 F}{\partial y^3} + (2+\nu) \frac{\partial^3 F}{\partial x^2 \partial y} = 0 \tag{2.21}$$

2.3 EFFECTIVE WIDTH DUE TO HARMONIC LOADING ON RIB

The bending moment induced in the beam due to the loading is expressed by means of the Fourier series. The rib is simply supported at $x = 0$ and $x = L$. The Fourier expression for the bending moment is

$$M(x) = \sum_{n=1,2,3...}^{\infty} a_n \sin\frac{n\pi}{L} x = \sum_{n=1,2,3...}^{\infty} a_n \sin\alpha_n x \qquad (2.22)$$

Since $\frac{d^2M(x)}{dx^2} = p(x)$, each term $a_n \sin\alpha_n x$ of the bending moment can be associated with a sine loading $p(x)$.

If we now consider σ_x for each individual Fourier term n only, then in Eqns. (2.13) and (2.14), the summation sign disappears and the effective width for each harmonic reduces to

$$b_e = \frac{\left.\frac{df_n}{dy}\right|_o^b}{\left(\frac{d^2 f_n}{dy^2}\right)_b} \qquad (2.23)$$

or

$$b_{es} = \frac{\left(\frac{df_{ns}}{dy}\right)_{y=b}}{\left(\frac{d^2 f_{ns}}{dy^2}\right)_{y=b}} \qquad (2.24)$$

When the constants A_n and B_n are incorporated, the above equations show that the effective width b_e for each individual harmonic n is independent of x and is constant along the span L.

If the loading $p(x)$ on both the ribs (Fig. 2.3) is of equal intensity, σ_x is symmetric along the y-direction. Hence, from Eqn. (2.9)

$$F_{ns} = (A_n \cosh\alpha_n y + B_n y \sinh\alpha_n y)\sin\alpha_n x$$

Imposing the boundary condition (2.21), we obtain for each term

$$A_n\alpha_n \sinh\alpha_n b + B_n(3 \sinh\alpha_n b + \alpha_n b \cosh\alpha_n b) -$$

$$- (2+\nu)[A_n\alpha_n \sin\alpha_n b + B_n(\sinh\alpha_n b + \alpha_n b \cosh\alpha_n b)] = 0$$

On simplification

$$A_n = B_n \frac{1}{\alpha_n}\left(\frac{1-\nu}{1+\nu} - \alpha_n b \coth\alpha_n b\right) \qquad (2.25)$$

It follows that

$$\left(\frac{df_{ns}}{dy}\right)_b = B_n \frac{2}{1+\nu} \sinh\alpha_n b$$

and

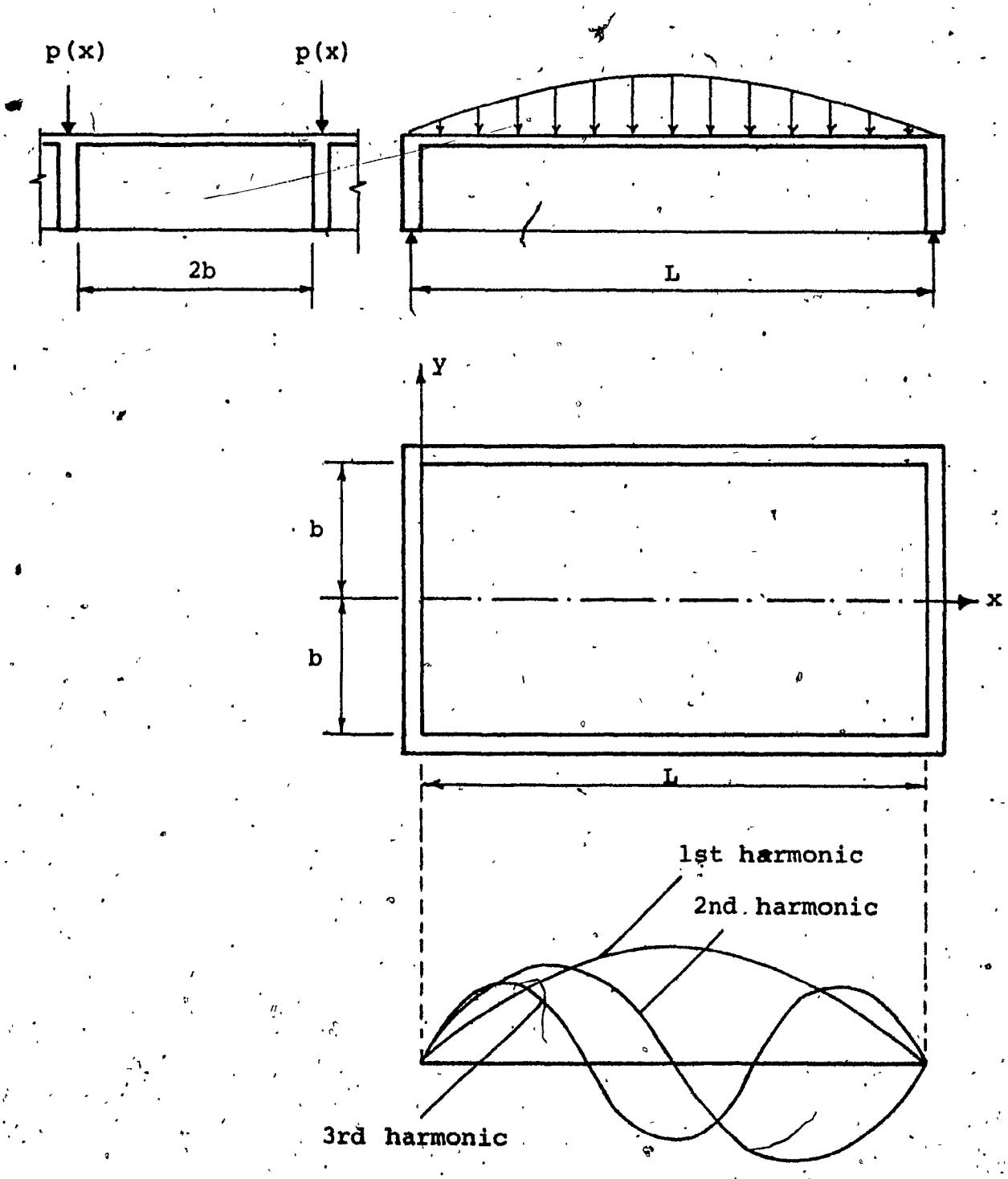

FIG. 2.3 T-Beam with Harmonic Loading on Rib

$$\left(\frac{d^2 f_{ns}}{dy^2}\right)_b = B_n \frac{\alpha_n}{2\sinh\alpha_n b}\left(\frac{3+\nu}{1+\nu}\sinh\alpha_n b - 2\alpha_n b\right)$$

Hence the effective width

$$b_{es} = \frac{\frac{1}{\alpha_n}\frac{4}{1+\nu}\sinh^2\alpha_n b}{\frac{3+\nu}{1+\nu}\sinh 2\alpha_n b - 2\alpha_n b} = L\frac{2(\cosh 2\alpha_n b - 1)}{n\pi[(3+\nu)\sinh 2\alpha_n b - 2(1+\nu)\alpha_n b]} \tag{2.26}$$

$$= b\frac{2(\cosh 2\alpha_n b - 1)}{\alpha_n b[(3+\nu)\sinh 2\alpha_n b - 2(1+\nu)\alpha_n b]} \tag{2.27}$$

The limiting values are as follows:

(i) For a flange plate that is very wide compared to the span L, Eqn. (2.26) gives for

$$\frac{b}{L} \to \infty, \qquad b_{es} \to \frac{2}{3+\nu}\cdot\frac{L}{n\pi} \tag{2.28}$$

(ii) If the span L is large compared to the flange width, it follows from (2.27) that for

$$\frac{b}{L} \to 0, \qquad b_{es} \to b \tag{2.29}$$

It is to be noted that the constant B_n, which serves to satisfy the strain compatibility of rib and plate at the contact line K, vanishes in Eqns. (2.26) and (2.27). Clearly, then, the effective width b_{es} for the n-th harmonic of the bending moment depends only on the span L and the rib spacing b.

2.4 FLANGE STRESS DUE TO HARMONIC LOADING ON RIB

To obtain the stress distribution in the flange plate it is necessary first to determine σ_{xb}, the longitudinal stress at the contact line K between the plate and the rib. Once σ_{xb} is derived, simple relations can be established for the distribution along the y-direction.

It follows from Eqns. (2.26) and (2.27) that for a particular harmonic, the effective width b_e is constant along the length of the beam but gets smaller as n increases. In Fig. 2.4, the beam is symmetrically loaded with the bending moment $M = M_o \sin \alpha_n x$. Clearly, the bending stress at the midspan

$$\sigma_{oxb} = \frac{M_o}{Z_{be}} \tag{2.30}$$

where Z_{be} is the section modulus. In computing Z_{be}, the actual flange width b is replaced by an effective width b_{es} for which the stress σ_{oxb} is constant. Eqn. (2.30) is valid for points at which the bending moment for each harmonic n is maximum, i.e., in general, at $x = \frac{L}{2n}$. The stress σ_{xb} at any arbitrary x is

$$\sigma_{xb} = \sigma_{oxb} \sin \alpha_n x$$

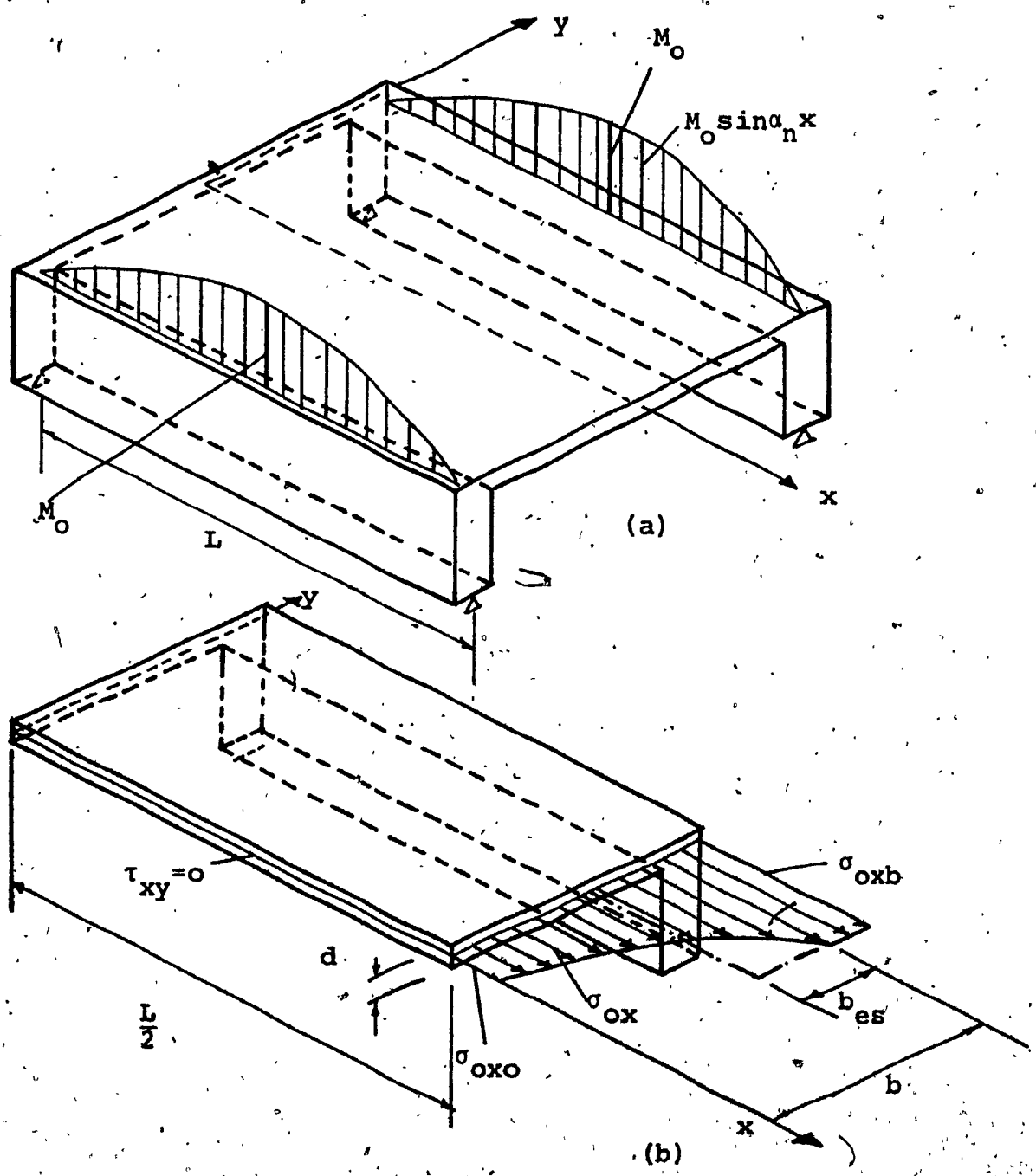

FIG.2.4 Symmetric Harmonic Moment Along Ribs

Substituting

$$C_{ns} = \left(\frac{1-\nu}{1+\nu} - \alpha_n b \coth\alpha_n b\right)$$

in Eqn. (2.25)

$$A_n = B_n \frac{C_{ns}}{\alpha_n}$$

The stress function (2.9) can then be expressed as

$$F_{ns} = B_n\left(\frac{C_{ns}}{\alpha_n}\cosh\alpha_n y + y\sinh\alpha_n y\right)\sin\alpha_n x$$

On differentiation

$$\sigma_x = \frac{\partial^2 F}{\partial y^2} = B_n\alpha_n[(C_{ns}+2)\cosh\alpha_n y + y\alpha_n\sinh\alpha_n y]\sin\alpha_n x$$

At $x = \frac{L}{2n}$ and $y = b$, one obtains

$$\sigma_{xb} = B_n\alpha_n\ [(C_{ns}+2)\cosh\alpha_n b + \alpha_n b\sinh\alpha_n b]$$

Simplifying,

$$\sigma_{xb} = B_n\frac{\alpha_n}{\sinh\alpha_n b}\left(\frac{3+\nu}{1+\nu}\cosh\alpha_n b\sinh\alpha_n b - \alpha_n b\right)$$

or

$$B_n = \frac{\sigma_{xb}}{\alpha_n} \frac{\sinh\alpha_n b}{\frac{3+\nu}{1+\nu}\cosh\alpha_n b \sinh\alpha_n b - \alpha_n b}$$

Hence

$$F_{ns} = \frac{\sigma_{xb}}{\alpha_n} \frac{(\frac{C_{ns}}{\alpha_n}\cosh\alpha_n y + y\sinh\alpha_n y)\sinh\alpha_n b}{\frac{3+\nu}{1+\nu}\cosh\alpha_n b \sinh\alpha_n b - \alpha_n b} \sin\alpha_n x \quad (2.31)$$

$$\sigma_x = \sigma_{xb} \frac{[(C_{ns}+2)\cosh\alpha_n y + y\alpha_n \sinh\alpha_n y]\sinh\alpha_n b}{\frac{3+\nu}{1+\nu}\cosh\alpha_n b \sinh\alpha_n b - \alpha_n b} \sin\alpha_n x \quad (2.32)$$

$$\sigma_y = -\sigma_{xb}\alpha_n \frac{(\frac{C_{ns}}{\alpha_n}\cosh\alpha_n y + y\sinh\alpha_n y)\sinh\alpha_n b}{\frac{3+\nu}{1+\nu}\cosh\alpha_n b \sinh\alpha_n b - \alpha_n b} \sin\alpha_n x \quad (2.33)$$

2.5 PROCEDURE TO COMPUTE STRESSES IN THE FLANGE

The basis for determining the stress in the flange plate lies in computing the σ_x for each individual harmonic of the bending moment and then summing them up to obtain the desired distribution.

From the dimensions of the T-beam shown in Fig. 2.5, the following parameters are first determined

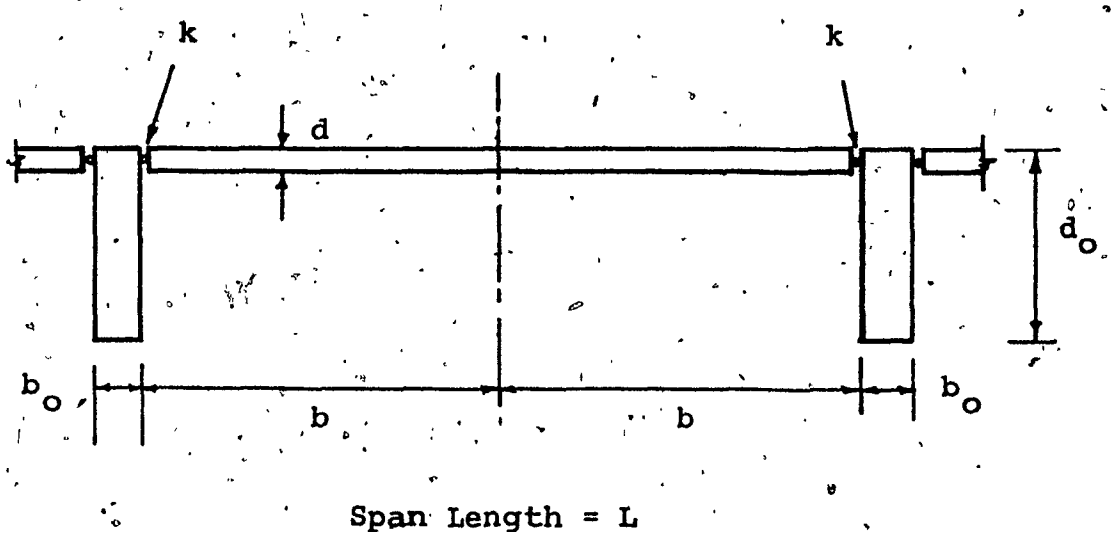

FIG. 2.5 Sectional Parameters of T-Beam

$$\delta = \frac{d}{d_o}$$

$$\beta = \frac{b}{b_o/2} = \frac{2b}{b_o} \qquad (2.34)$$

$$\gamma = \frac{2b}{L}$$

A systematic procedure for computing the stresses will be described for an example case of distributed load on the beam. The bending moment in the beam is first expressed as a Fourier sine series

$$M_o(\xi) = \overline{M}_o(\xi)pL^2 = pL^2 \sum_{n=1}^{\infty} \overline{M}_n(\xi) = pL^2 \sum_{n=1}^{\infty} a_n \sin(n\pi\xi) \qquad (2.35)$$

where $\xi = \frac{x}{L}$

From Eqn. (2.27), the constant effective width for the n-th harmonic is obtained as

$$b_{esn} = b\,\frac{2}{\alpha_n b}\,\frac{\cosh(2\alpha_n b) - 1}{(3+\nu)\sinh(2\alpha_n b) - 2(1+\nu)\alpha_n b}$$

Substitution of $\alpha_n = \frac{n\pi}{L}$ and $\gamma = \frac{2b}{L}$, yields

$$\lambda_n = \frac{b_{esn}}{b} = \frac{4}{n\pi\gamma} \frac{\cosh(n\pi\gamma - 1)}{(3+\nu)\sinh(n\pi\gamma) - (1+\nu)n\pi\gamma}$$

Assuming Poisson's ratio

$$\nu = \frac{1}{6}$$

$$\lambda_n = \frac{24}{n\pi\gamma} \frac{\cosh(n\pi\gamma) - 1}{19\sinh(n\pi\gamma) - 7(n\pi\gamma)} \tag{2.36}$$

The section modulus for the rib only is

$$Z_o = \frac{b_o d_o^2}{6}$$

Referring to the contact line K, the section modulus of the T-section for the n-th harmonic can be expressed as

$$Z_{kn} = \eta_n Z_o \tag{2.37}$$

where

$$\eta_n = \frac{1}{1-\delta}\left[(1+\lambda_n\beta\delta)(1+\lambda_n\beta\delta^3) + 3\lambda_n\beta\delta(1-\delta)^2\right]$$

Longitudinal stress at line K, then is

$$\sigma_{xbn}(\xi) = \frac{M_n}{Z_{kn}} = \frac{pL^2}{Z_o} \cdot \frac{\overline{M}_n}{\eta_n} = \frac{pL^2}{Z_o} \cdot \frac{1}{\eta_n} a_n \sin(n\pi\xi) \tag{2.38}$$

Since the effective flange width for the n-th harmonic is already known from Eqn. (2.36), the corresponding compressive force per unit thickness of the flange is

$$C_n(\xi) = \sigma_{xbn}\, b_{esn}$$

The summation of individual $\sigma_{xbn}(\xi)$ and $C_n(\xi)$ yields the maximum stress $\bar{\sigma}_{xb}$ and the corresponding compressive force.

$$\bar{\sigma}_{xb}(\xi) = \sum_{n=1}^{\infty} \sigma_{xbn}(\xi)$$

$$C(\xi) = \sum_{n=1}^{\infty} C_n(\xi)$$

By the definition of effective width, it follows that for a given ξ

$$\bar{\sigma}_{xb}\, b_e = \sum \sigma_{xbn}\, b_{en}$$

or (2.40)

$$b_e = \frac{1}{\bar{\sigma}_{xb}} \sum \sigma_{xbn}\, b_{en}$$

Once σ_{xbn} is determined from Eqn. (2.38), the distribution of σ_x along the y-direction can be easily obtained using Eqn. (2.32).

The expressions above for σ_x have been derived for the middle surface of the flange plate, i.e., at the contact line K. To obtain the stresses at the top and bottom fibres of the T-section, corresponding section moduli are used.

These are, for top and bottom respectively,

$$Z_t = Z_o \eta_t$$

$$Z_b = Z_o \eta_b$$

where

$$\eta_t = \frac{(1+\lambda\beta\delta)(1+\lambda\beta\delta^3) + 3\lambda\beta\delta(1-\delta)^2}{1 + \lambda\beta\delta^2}$$

and

$$\eta_b = \frac{(1+\lambda\beta\delta)(1+\lambda\beta\delta^3) + 3\lambda\beta\delta(1-\delta)^2}{1 + \lambda\beta\delta(2 - \delta)}$$

Hence, for each harmonic, the stresses at the top and bottom fibres of the web are

$$\sigma_{xbn}^{top} = -\frac{M_n(\xi)}{Z_t}$$

$$\sigma_{xn}^{bot} = \frac{M_n(\xi)}{Z_b} \qquad (2.41)$$

The above procedure has been used to determine the stress distribution for the test beams described below.

2.6 ANALYSIS OF THE EXAMPLE BEAMS

Three simply supported T-beams with different cross-sectional dimensions have been analyzed for a uniformly distributed load of p = 1000 lbs per linear foot. The flange widths have been varied to study the variation of longitudinal stress in the flange along the width. The dimensions and loading are shown in Figs. 2.6 and 2.7. The bending moment for the beam is expressed as a Fourier sine series

$$M(\xi) = \frac{pL^2}{2}(\xi-\xi^2)$$

$$= \frac{pL^2}{2}\sum_{n=1}^{\infty} \bar{M}_n(\xi)$$

$$= \frac{pL^2}{2}\sum_{n=1}^{\infty} a_n \sin(n\pi\xi)$$

The constant $a_n = \dfrac{4(1-\cos n\pi)}{n^3\pi^3}$ and

$$M(\xi) = \frac{pL^2}{2}\sum_{n=1,3,5\ldots}^{\infty} \frac{4(1-\cos n\pi)}{n^3\pi^3}\sin(n\pi\xi)$$

$$= \frac{4pL^2}{\pi^3}\sum_{n=1,3,5\ldots}^{\infty} \frac{1}{n^3}\sin(n\pi\xi)$$

Following the procedure in Section 2.5, a small computer program was written to calculate the longitudinal stress σ_x in the flange plate at midspan, i.e. $\xi = \frac{x}{L} = 0.5$.

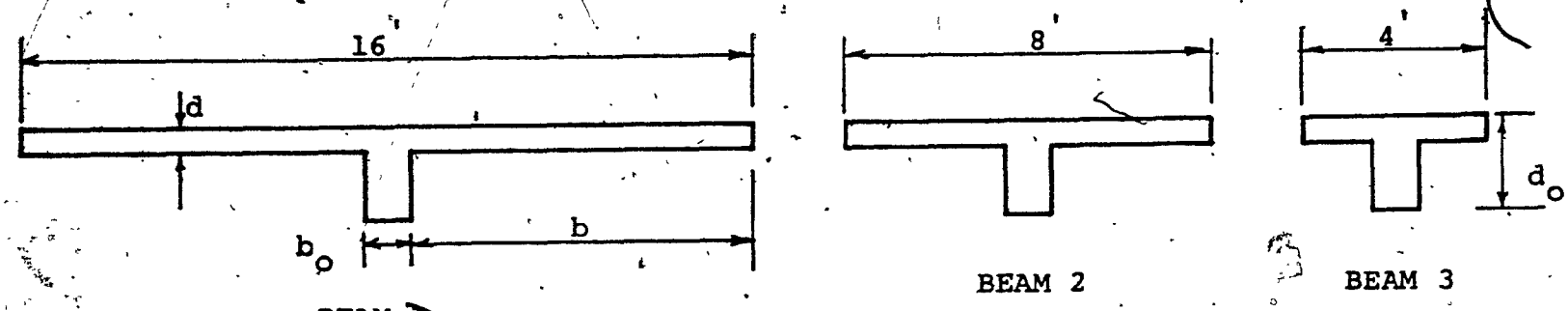

BEAM 1

	BEAM 1	BEAM 2	BEAM 3
b	89 in.	41 in.	17 in.
d	6 "	6 "	6 "
d_o	24 "	24 "	24 "
b_o	14 "	14 "	14 "
L	180 "	180 "	180 "
$\delta = \frac{d}{d_o}$	0.25	0.25	0.25
$\beta = \frac{2b}{b_o}$	12.83	5.857	2.428
$\gamma = \frac{2b}{L}$	0.989	0.456	0.189

FIG. 2.6 Dimensions of Test Beams

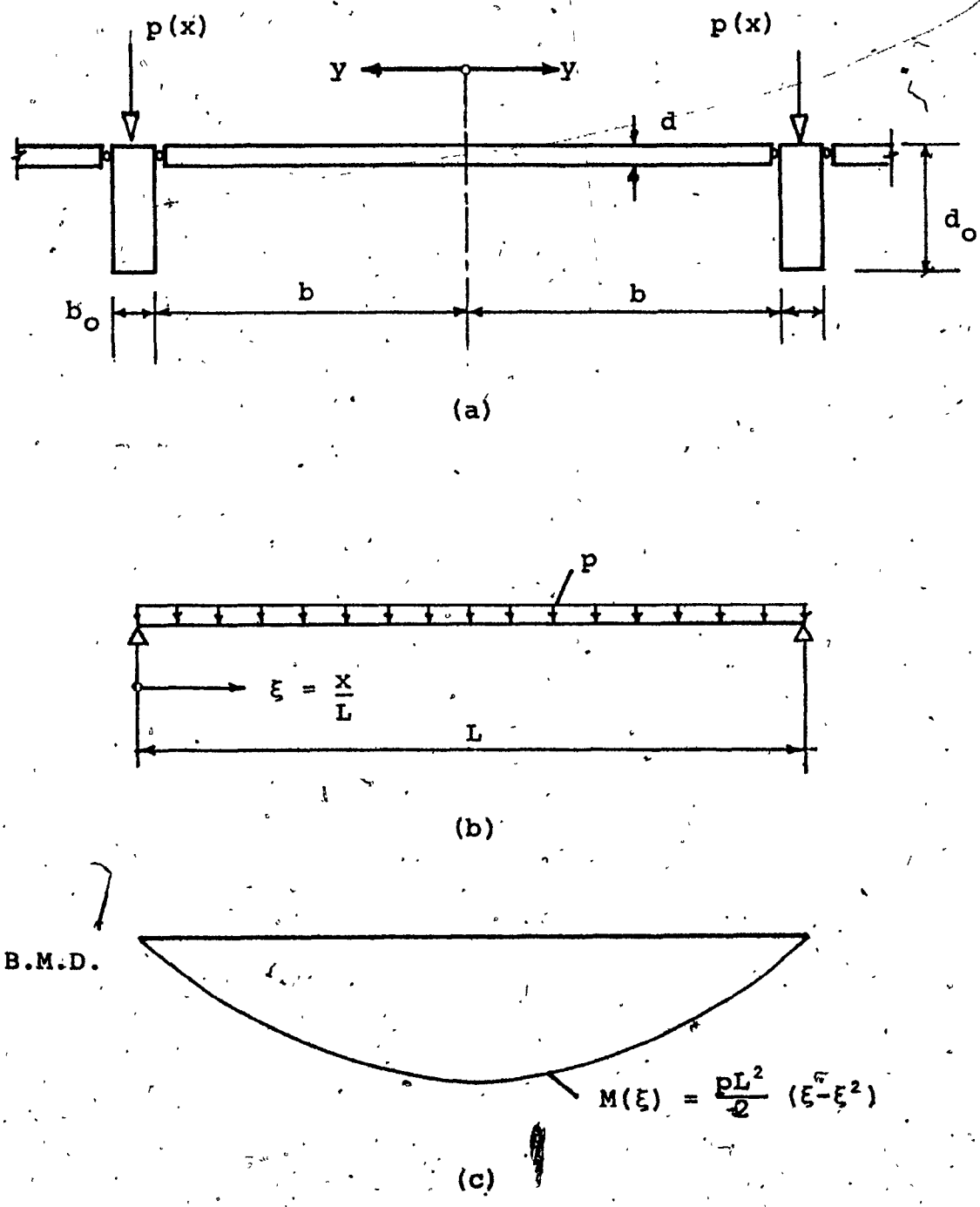

FIG. 2.7 Loading on Test Beams

For each harmonic n, the stress at the midsurface of the plate is obtained from Eqn. (2.38) as

$$\sigma_{xbn} = \frac{4pL^2}{\pi^3} \cdot \frac{1}{z_o \eta_n} \cdot \frac{1}{n^3} \sin\left(\frac{n\pi}{2}\right)$$

Summation was done for twenty harmonics only. Eqn. (2.32) was used to compute the distribution of σ_x along the y-axis. The effective width b_e has also been calculated from Eqn. (2.40). Finally, stress distribution at the top fibre of the T-section is determined using Eqn. (2.41). Stresses at the bottom surface are obtained by linear interpolation. The results are presented in Table 2.1.

TABLE 2.1

Longitudinal Stresses σ_x in the Flange Plate at Midspan - Classical Method

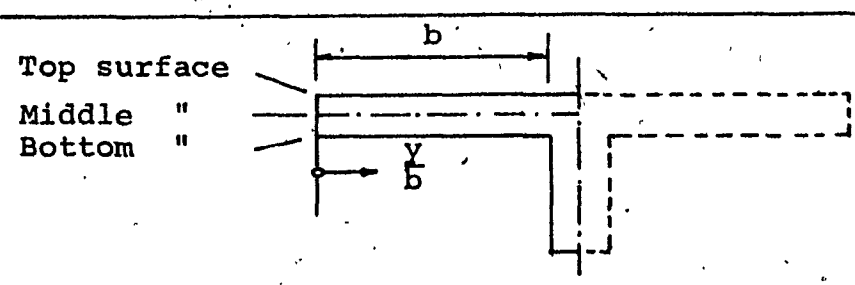

		$\frac{y}{b}$					
		0.0	.2	.4	.6	.8	1.0
BEAM 1	Top	-12.4	-14.1	-19.7	-29.9	-45.8	-68.9
	Mid.	- 7.0	- 8.0	-11.1	-16.9	-25.7	-38.5
	Bot.	- 1.6	- 1.9	- 2.5	- 3.9	- 5.6	- 8.1
BEAM 2	Top	-49.7	-50.8	-54.1	-59.6	-67.3	-77.4
	Mid.	-29.3	-30.0	-31.9	-35.0	-39.5	-45.4
	Bot.	- 8.9	- 9.2	- 9.7	-10.4	-11.7	-13.4
BEAM 3	Top	-101.9	-102.3	-103.3	-104.9	-107.2	-110.2
	Mid.	- 66.8	- 67.1	- 67.7	- 68.8	- 70.3	- 72.2
	Bot.	- 31.7	- 31.9	- 32.1	- 32.7	- 33.4	- 34.2

Note: Stresses are in psi
"-" compression
"+" tension

CHAPTER 3

FINITE ELEMENT METHOD

CHAPTER 3

FINITE ELEMENT METHOD

3.1 GENERAL

In the last fifteen years, the development of the finite element method has been almost explosive. With the availability of high-speed electronic computers and with the growing interest in numerical methods of engineering analysis, the finite element technique has proven to be an extremely powerful tool for solving problems of complex geometries and loading, where solution by the classical methods become impossible. Although originally developed for structural analysis, the method has been successfully extended to other fields of engineering. Numerous works have been published on the development of the method. A comprehensive bibliography can be obtained in the textbooks [11,12,13,14,15]. Special purpose conferences [16,17] have been devoted exclusively to the application of the method.

The technique is based on the concept of replacing the actual continuum by a mathematical model made up of structural elements of finite size. Various elements have been developed for the solution of problems in the fields of two or three-dimensional elasticity. The analysis in this dissertation uses a three-dimensional solid element. Clough [16] has made a comparative study of the relative merits of various

tetrahedron and hexahedron elements. The important conclusion was that the 20-node isoparametric hexahedron is vastly superior, with regard to its structural properties, and also in terms of its general applicability.

The isoparametric element concept has been advanced by Irons, Zienkiewicz and Ergatoudis [18,19]. In this type of element, the displacements and the geometry are described in terms of the same parameters. Hence, the name isoparametric. Thus, if the displacement field is a quadratic polynomial, the faces of the element are described by the same functions.

The main objective in using isoparametric elements for structural idealization is to achieve a given level of solution accuracy with the smallest number of degrees of freedom. This is particularly important in the analysis of solids, where three-dimensional idealization introduces a vast number of degrees of freedom in the conventional finite element approach. Elements based on rectangular brick offer the advantages of simple geometry and improved properties. One of the refined extensions of the brick is the 20-noded element with quadratic edge. A better modelling of curved boundaries can, thus, be achieved with such elements. In order to prescribe quadratic variation uniquely, one additional node on each side is needed. The presence of mid-side nodes, however, tends to increase the bandwidth of the equation system, which in turn, increases the computational effort for a solution.

One of the ways to reduce this effort is to formulate elements with less numbers of nodes, but with a larger number of degrees of freedom at each node. The resulting overall stiffness matrix for the structure will then have a narrow bandwidth. A fuller discussion of the various types of elements is beyond the scope of this work. In this dissertation, the 20-noded isoparametric hexahedron is used. For the sake of completeness, the formulation of this element is described in detail.

3.2 FORMULATION OF THE 20-NODE ISOPARAMETRIC HEXAHEDRON

The first step in the formulation of the element stiffness matrix is the selection of a suitable set of shape functions to define the variation of displacement components in terms of the nodal values of these functions. A shape function, also known as the interpolation function, may be defined as a displacement pattern having the value of unity at one node and zero at all the other nodes.

The shape functions are specified in local coordinates, α, β, γ with the origin of the system at the centroid of the element, as shown in Fig. 3.1. This local coordinate system is such that the element is bounded by faces with coordinate values $\alpha = \pm 1$, $\beta = \pm 1$, $\gamma = \pm 1$. Thus, in the local coordinates, the element is a cube with mid-edge nodes. In the global coordinates, however, the position of all nodes is

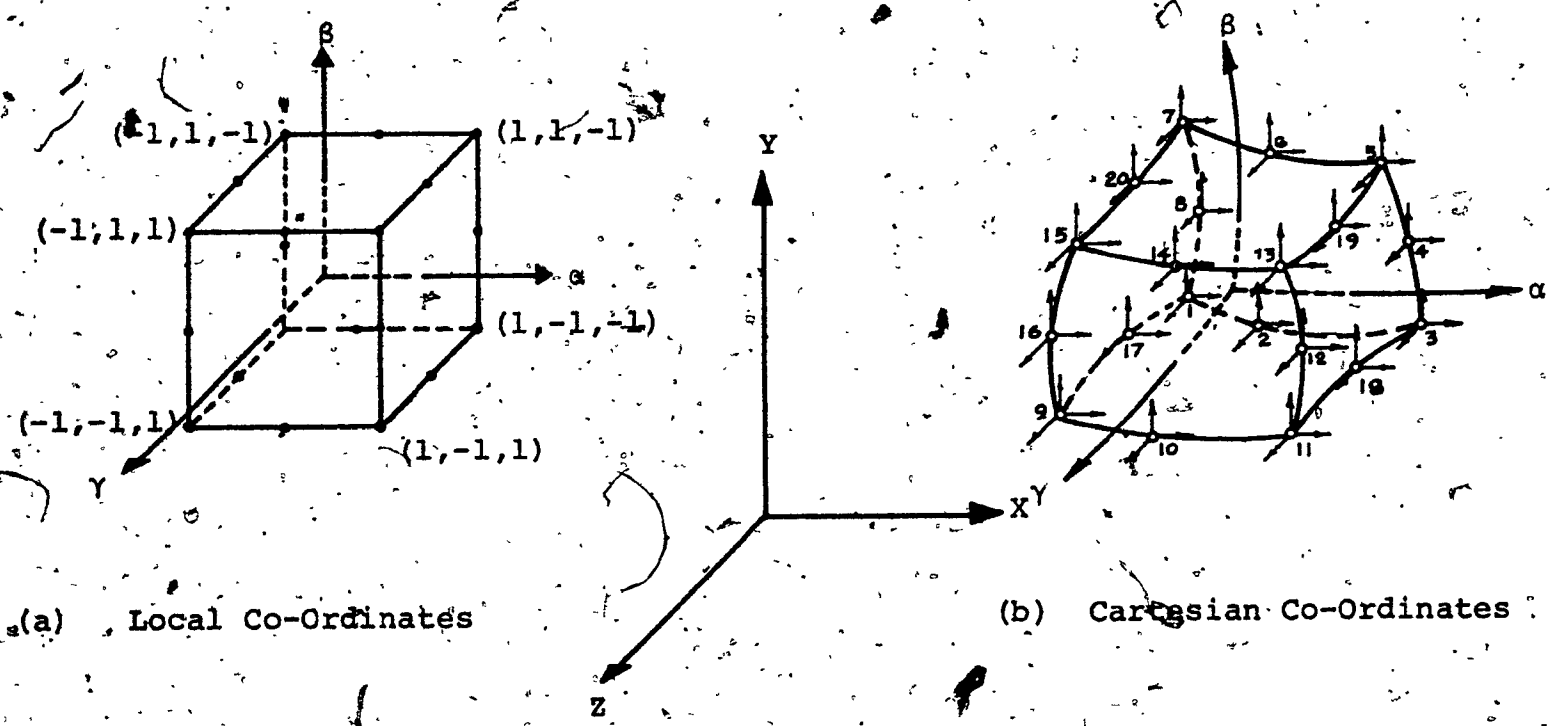

(a) Local Co-Ordinates

(b) Cartesian Co-Ordinates

FIG. 3.1 20 Node Isoparametric Hexahedron

arbitrary; only the topology of the cube is retained. Each edge of the hexahedron is a quadratic curve in space defined by the positions of the three nodes associated with the edge.

The relationship between the local and global Cartesian coordinates is

$$
\begin{aligned}
x &= \sum_{i=1}^{20} N_i x_i \\
y &= \sum_{i=1}^{20} N_i y_i \qquad (3.1) \\
z &= \sum_{i=1}^{20} N_i z_i
\end{aligned}
$$

where x_i, y_i, z_i are the coordinates of the i-th node of the hexahedron in the global system. The quadratic shape functions N_i, for the nodal numbering scheme of Fig. 3.1, are given by

$$
\left.
\begin{aligned}
N_i &= \frac{1}{8}(1 + \alpha\alpha_i)(1 + \beta\beta_i)(1 + \gamma\gamma_i)(\alpha\alpha_i + \beta\beta_i + \gamma\gamma_i - 2) \\
\text{for} \quad i &= 1, 3, 5, 7, 9, 11, 13, 15 \\
N_i &= \frac{1}{4}(1 - \alpha^2)(1 + \beta\beta_i)(1 + \gamma\gamma_i) \\
\text{for} \quad i &= 2, 6, 10, 14
\end{aligned}
\right\} \qquad (3.2)
$$

$$\left.\begin{aligned} N_i &= \frac{1}{4}(1 + \alpha\alpha_i)(1 - \beta^2)(1 + \gamma\gamma_i) \\ \text{for} \quad i &= 4,\ 12,\ 14,\ 16 \\ N_i &= \frac{1}{4}(1 + \alpha\alpha_i)(1 + \beta\beta_i)(1 - \gamma^2) \\ \text{for} \quad i &= 17,\ 18,\ 19,\ 20 \end{aligned}\right\} \qquad (3.2)$$

The equation system (3.1) can be written in matrix form as

$$\begin{Bmatrix} x \\ y \\ z \end{Bmatrix} = \begin{bmatrix} \{N\}^T & \{0\}^T & \{0\}^T \\ \{0\}^T & \{N\}^T & \{0\}^T \\ \{0\}^T & \{0\}^T & \{N\}^T \end{bmatrix} \begin{Bmatrix} \{x_n\} \\ \{y_n\} \\ \{z_n\} \end{Bmatrix} \qquad (3.3)$$

where

$$\{N\}^T = [N_1 \quad N_2 \ \ldots\ldots\ldots N_{20}]$$

and

$$\{x_n\}^T = [x_1 \quad x_2 \ \ldots\ldots\ldots x_{20}]$$

The hexahedron element has three generalized displacements at each of the nodes. These are the three displacement components u, v, w in the X, Y, Z directions, respectively. The functional representations are

$$u = \sum_{i=1}^{20} N_i u_i$$

$$v = \sum_{i=1}^{20} N_i v_i \qquad (3.4)$$

$$w = \sum_{i=1}^{20} N_i w_i$$

where u_i, v_i, w_i are the displacements of the i-th node. It is noted that identical shape functions N_i are used to describe the element geometry and the nodal displacements. Eqs. (3.4) are conveniently expressed as

$$\begin{Bmatrix} u \\ v \\ w \end{Bmatrix} = \begin{bmatrix} N_1 & 0 & 0 & N_2 & 0 & 0 \ldots N_{20} & 0 & 0 \\ 0 & N_1 & 0 & 0 & N_2 & 0 \ldots 0 & N_{20} & 0 \\ 0 & 0 & N_1 & 0 & 0 & N_2 \ldots 0 & 0 & N_{20} \end{bmatrix} \{q\}$$

$$= [N]\{q\} \qquad (3.5)$$

where

$$\{q\}^T = [u_1 \;\; v_1 \;\; w_1 \;\; u_2 \;\; v_2 \;\; w_2 \;\; \ldots u_{20} \;\; v_{20} \;\; w_{20}]$$

By definition, the strains in a three-dimensional solid are given by the derivatives of the displacements:

$$\begin{Bmatrix} \varepsilon_x \\ \varepsilon_y \\ \varepsilon_z \\ \gamma_{xy} \\ \gamma_{yz} \\ \gamma_{zx} \end{Bmatrix} = \begin{Bmatrix} \dfrac{\partial u}{\partial x} \\ \dfrac{\partial v}{\partial y} \\ \dfrac{\partial w}{\partial z} \\ \dfrac{\partial u}{\partial y} + \dfrac{\partial v}{\partial x} \\ \dfrac{\partial v}{\partial z} + \dfrac{\partial w}{\partial y} \\ \dfrac{\partial w}{\partial x} + \dfrac{\partial u}{\partial z} \end{Bmatrix} \tag{3.6}$$

By differentiating Eq. (3.4) appropriately, the strains can be expressed in terms of the nodal displacements as:

$$\{\varepsilon\} = [\ [B_1][B_2]\ \ldots\ldots\ldots[B_{20}]\ ]\{q\} = [B]\{q\} \tag{3.7}$$

where

$$[B_i] = \begin{bmatrix} \dfrac{\partial Ni}{\partial x} & 0 & 0 \\ 0 & \dfrac{\partial Ni}{\partial y} & 0 \\ 0 & 0 & \dfrac{\partial Ni}{\partial z} \\ \dfrac{\partial Ni}{\partial y} & \dfrac{\partial Ni}{\partial x} & 0 \\ 0 & \dfrac{\partial Ni}{\partial z} & \dfrac{\partial Ni}{\partial y} \\ \dfrac{\partial Ni}{\partial z} & 0 & \dfrac{\partial Ni}{\partial x} \end{bmatrix}$$

From Eq. (3.7), it is seen that the [B] matrix contains the first derivatives of the shape functions with respect to the global coordinates. N_i is defined in terms of the local coordinates α, β, γ and there are no explicit

equations for α, β, γ in terms of x, y, z. Hence, to obtain the required derivatives the chain rule of differentiation is employed in an inverse sense, as follows:

$$\begin{Bmatrix} \frac{\partial Ni}{\partial \alpha} \\ \frac{\partial Ni}{\partial \beta} \\ \frac{\partial Ni}{\partial \gamma} \end{Bmatrix} = \begin{bmatrix} \frac{\partial x}{\partial \alpha} & \frac{\partial y}{\partial \alpha} & \frac{\partial z}{\partial \alpha} \\ \frac{\partial x}{\partial \beta} & \frac{\partial y}{\partial \beta} & \frac{\partial z}{\partial \beta} \\ \frac{\partial x}{\partial \gamma} & \frac{\partial y}{\partial \gamma} & \frac{\partial z}{\partial \gamma} \end{bmatrix} \begin{Bmatrix} \frac{\partial Ni}{\partial x} \\ \frac{\partial Ni}{\partial y} \\ \frac{\partial Ni}{\partial z} \end{Bmatrix} = [J] \begin{Bmatrix} \frac{\partial Ni}{\partial x} \\ \frac{\partial Ni}{\partial y} \\ \frac{\partial Ni}{\partial z} \end{Bmatrix} \tag{3.8}$$

The derivatives in the local coordinates appearing on the left-hand side of the above equation can be evaluated from the relations (3.2). Since x, y, z are explicitly given by the geometric relations (3.1), the matrix [J] can be found explicitly in terms of the local coordinates. The square matrix [J] is called the Jacobian matrix. Hence, the terms required in the strain matrix [B] are found from Eq. (3.8).

$$\begin{Bmatrix} \frac{\partial Ni}{\partial x} \\ \frac{\partial Ni}{\partial y} \\ \frac{\partial Ni}{\partial z} \end{Bmatrix} = [J]^{-1} \begin{Bmatrix} \frac{\partial Ni}{\partial \alpha} \\ \frac{\partial Ni}{\partial \beta} \\ \frac{\partial Ni}{\partial \gamma} \end{Bmatrix} \tag{3.9}$$

The 3 x 3 Jacobian matrix [J] is obtained numerically from

$$\underset{3 \times 3}{[J]} = \underset{3 \times 20}{\begin{bmatrix} \frac{\partial N_1}{\partial \alpha} & \frac{\partial N_2}{\partial \alpha} & \cdots & \frac{\partial N_{20}}{\partial \alpha} \\ \frac{\partial N_1}{\partial \beta} & \frac{\partial N_2}{\partial \beta} & \cdots & \frac{\partial N_{20}}{\partial \beta} \\ \frac{\partial N_1}{\partial \gamma} & \frac{\partial N_2}{\partial \gamma} & \cdots & \frac{\partial N_{20}}{\partial \gamma} \end{bmatrix}} \underset{20 \times 3}{\begin{bmatrix} x_1 & y_1 & z_1 \\ x_2 & y_2 & z_2 \\ \vdots & \vdots & \vdots \\ x_{20} & y_{20} & z_{20} \end{bmatrix}} \tag{3.10}$$

The stress-strain relationship for an elastic solid may be written as

$$\begin{Bmatrix} \sigma_x \\ \sigma_y \\ \sigma_z \\ \tau_{xy} \\ \tau_{yz} \\ \tau_{zx} \end{Bmatrix} = \{\sigma\} = [D]\{\varepsilon\} \tag{3.11}$$

where $\{\sigma\}$ is the stress vector corresponding to the strains $\{\varepsilon\}$, and for an isotropic material

$$[D] = \frac{E}{(1+\nu)(1-2\nu)} \begin{bmatrix} 1-\nu & \nu & \nu & 0 & 0 & 0 \\ \nu & 1-\nu & \nu & 0 & 0 & 0 \\ \nu & \nu & 1-\nu & 0 & 0 & 0 \\ 0 & 0 & 0 & \frac{1-2\nu}{2} & 0 & 0 \\ 0 & 0 & 0 & 0 & \frac{1-2\nu}{2} & 0 \\ 0 & 0 & 0 & 0 & 0 & \frac{1-2\nu}{2} \end{bmatrix}$$

The element stiffness matrix may now be formulated from the strain energy relationship and is expressed in the general form [12,13]

$$[k] = \int_V [B]^T [D][B] \, dV \qquad (3.12)$$

Since the strain matrix [B] is expressed in local coordinates α, β, γ, it is necessary to carry out the integration in the local coordinate space, which involves the determinant of the Jacobian matrix [J]. Thus, a differential volume element

$$dV = dxdydz = \det [J] \, d\alpha d\beta d\gamma \qquad (3.13)$$

Hence, Eq. (3.12) becomes

$$[K] = \int_{-1}^{1}\int_{-1}^{1}\int_{-1}^{1} [B]^T [D][B] \det [J] \, d\alpha d\beta d\gamma \qquad (3.14)$$

Explicit form of the integral above is of a complex nature and numerical integration is required. An efficient method of performing this integration is to use Gaussian quadrature.

If a function $f(x)$ is to be integrated between the limits $[-1, 1]$, then the approximate value of the integral can be found by replacing the integrand as follows

$$\int_{-1}^{1} f(x)\, dx = \sum_{j=1}^{N} w_j f(a_j)$$

where w_j are the weighting coefficients, $f(a_j)$ the value of the functions at specified points a_j and N the number of Gaussian points. Tables of Gauss points and weight coefficients can be found in textbooks on numerical methods. Hence, the stiffness matrix in Eq. (3.14) now becomes

$$[k] = \sum_{i=1}^{N} \sum_{j=1}^{N} \sum_{k=1}^{N} |J|_{ijk}\, w_i w_j w_k\, [B]^T [D][B] \qquad (3.15)$$

where $|J| = \det [J]$.

In this dissertation, $N = 3$ is used. It will be noted that $|J|$ and the terms in $[B]$ are all functions of the Gaussian integration points. The stress-strain matrix $[D]$ is assumed constant throughout the volume.

3.3 WORK EQUIVALENT NODAL FORCES

Since the stiffness method of analysis uses the force-displacement relations at the nodes, any distributed load on an element must be replaced by a set of nodal forces. In simpler elements these nodal forces are sometimes assigned intuitively. But for higher order elements, such as those used in this work, it is essential that joint loads be consistent with the energy principle employed to derive the element stiffness properties.

If a surface loading $p(x,y,z)$ acts on the surface S of the element, then the equivalent joint loads are found by equating the work done by the surface loading to the work done by the joint loads for an arbitrary set of nodal displacements on S. These loads are termed the work equivalent loads. It can be shown that for a surface loading, the joint loads are

$$\{Q\} = \int_S [N]^T \{p\}\, dS \qquad (3.16)$$

where $\{Q\}$ is the vector of the load components. Numerical integration is required to obtain the vector. For instance, Fig. 3.2 shows one rectangular face containing the eight nodes. If the pressure intensities at the nodes are $p_1, p_2, \ldots,$ then the work equivalent load vector for the element under discussion is given by the following matrix equation.

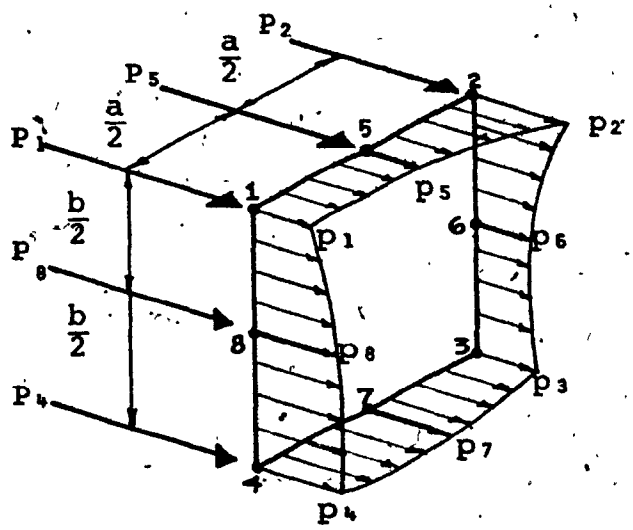

FIG. 3.2 Work Equivalent Nodal Forces

$$\begin{Bmatrix} P_1 \\ P_2 \\ P_3 \\ P_4 \\ P_5 \\ P_6 \\ P_7 \\ P_8 \end{Bmatrix} = \frac{ab}{180} \begin{bmatrix} 6 & 2 & 3 & 2 & -6 & -8 & -8 & -6 \\ 2 & 6 & 2 & 3 & -6 & -6 & -8 & -8 \\ 3 & 2 & 6 & 2 & -8 & -6 & -6 & -8 \\ 2 & 3 & 2 & 6 & -8 & -8 & -6 & -6 \\ -6 & -6 & -8 & -8 & 32 & 20 & 16 & 20 \\ -8 & -6 & -6 & -8 & 20 & 32 & 20 & 16 \\ -8 & -8 & -6 & -6 & 16 & 20 & 32 & 20 \\ -6 & -8 & -8 & -6 & 20 & 16 & 20 & 32 \end{bmatrix} \begin{Bmatrix} p_1 \\ p_2 \\ p_3 \\ p_4 \\ p_5 \\ p_6 \\ p_7 \\ p_8 \end{Bmatrix} \quad (3.17)$$

A similar procedure is used for body forces and thermal loads.

3.4 ASSEMBLY AND SOLUTION OF EQUILIBRIUM EQUATIONS

When all the element stiffness matrices $[k]$ and the corresponding load vectors $\{Q\}$ have been generated, they are then properly superposed to give the final set of equilibrium equations for the nodes of the entire structure. Concentrated loads, if any, are also assembled in the load vector. The equations can be represented in matrix form as

$$[K]\{\delta\} = \{F\}$$

where $[K]$ is the overall stiffness matrix of the structure, $\{F\}$ is the applied load vector and $\{\delta\}$ is the vector of displacements.

At this stage, known displacement boundary conditions are introduced into the equations and the system solved for the unknown displacements.

3.5 COMPUTATION OF STRESSES AND STRAINS

With the nodal displacements determined, the strains are found from Eq. (3.7)

$$\{\varepsilon\} = [B]\{q\}$$

where the matrix [B] is a function of the local coordinates α,β,γ at the point where the strains are to be evaluated. It will be noted that for each point in the body where the strains are to be computed, a separate matrix [B] is required.

Stresses are now found from the stress-strain relation (3.11)

$$\{\sigma\} = [D]\{\varepsilon\}$$

3.6 DESCRIPTION OF COMPUTER PROGRAM

The computer program developed for the three-dimensional finite element analysis is described very briefly. The system consists of three main line programs linked together and written in FORTRAN for a CDC6400 computer. For

intermediate data handling, auxiliary storage is used. Each individual program calls a number of subroutines which form the basic modules of the system. The flow chart in Table 3.1 shows the functions of the main phases of the program.

For the specific problem in this dissertation, a few special features have been introduced in the program, primarily to reduce the amount of input data, and secondly, to minimize the computational effort. For instance, the coordinates of only a few nodes are input, while the majority are generated automatically. Since numerical integration is required, the generation of stiffness matrixs can be time-consuming. If two or more elements are identical in all respects, the stiffness matrix is generated only once, thus saving computer time. Only the upper triangular part of the matrix is generated and stored in a vector form.

Various sequences of operations to obtain this matrix have been suggested in the literature [20]. The procedure used in this program consists of loops over all the Gauss points, each loop containing the following steps:

(1) Evaluate $\frac{\partial Ni}{\partial \alpha}$, etc., at the integration points.

(2) Form the Jacobian matrix [J] ; find its determinant and inverse.

(3) Form the [B] matrix.

TABLE 3.1

Flow Chart of the Computer Program

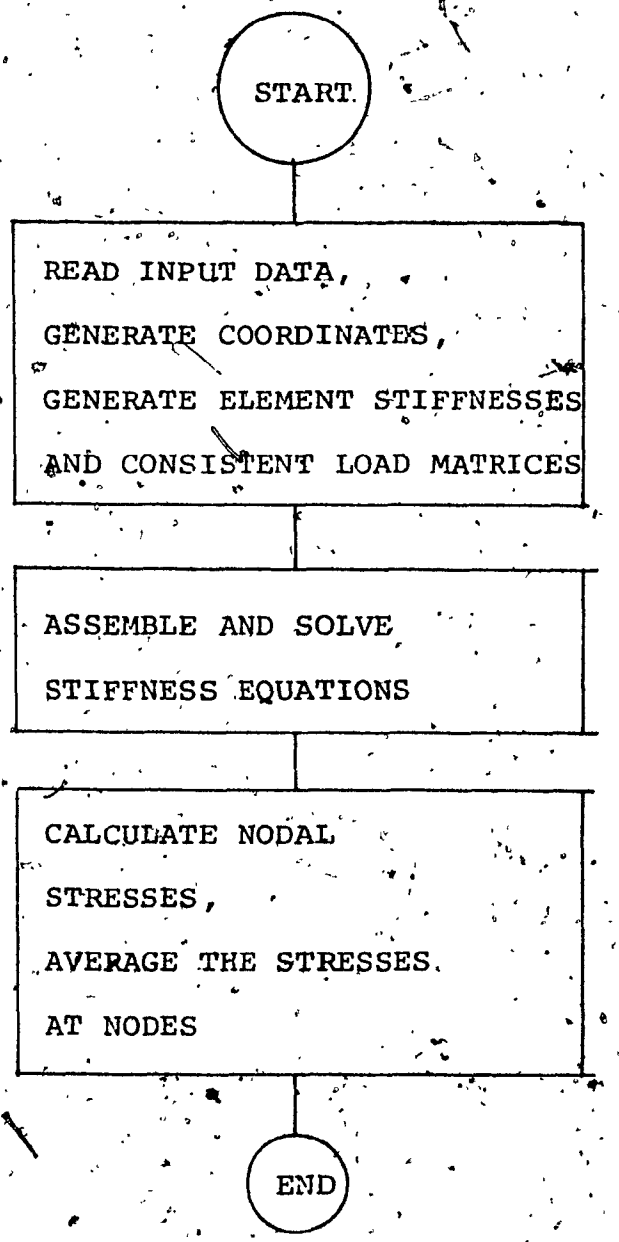

(4) Evaluate $[B]^T [D][B]$, and multiply each term by $|J|$ and by the corresponding weighting coefficient.

(5) Add to the stiffness matrix.

The solution procedure adopted in this program is based on the Gaussian elimination and is subject to a maximum semi-bandwidth. However, for efficiency, the assembly and elimination of the equations go hand-in-hand [12, 21, 22]. The stiffness equations for a node are eliminated as soon as they are completely formed. To achieve this end, the node numbers of an element are first sorted, to have the smallest node number as its first node. The elements are then ordered so that all the first node numbers are in sequential order. Thus, the assembly will stop automatically whenever the first node number of an element is larger than the node number that is currently being solved.

Having recovered the displacements, the stresses at the element nodes are then computed. Due to the fact that any one node may be common to a maximum of eight elements, an averaging procedure is used. The final stresses at a node are obtained as the average of the stresses calculated from all the elements connected to it.

3.7 TESTING OF THE COMPUTER PROGRAM

To verify the program, a number of sample problems have been successfully solved by the program. One of these is a simple cantilever loaded with uniform compression on its end face. The same problem was also solved by Marlon-Lambert et al [17] using the same element. The deflections, stresses and reactions obtained in this study are identical to theirs.

3.8 ANALYSIS OF SIMPLY SUPPORTED T-BEAMS

The three beams chosen for the finite element analysis are the same as those used in the classical treatment. The dimensions and loading are shown in Figs. 2.6 and 2.7. It will be noted that the uniform loading of 1000 lbs per ft is applied on the rib only. Due to symmetry, only a quarter of the three-dimensional configuration of the beam is analyzed using the hexahedron solid elements. The hatched area in Fig. 3.3, shows the portion analyzed. Finite element idealization consists of dividing this area into four segments, each segment being composed of five hexahedrons. The scheme is presented in Fig. 3.4. The total system, then, consists of 20 elements and 188 nodes, with 3 degrees of freedom at each node. Boundary conditions have also included constraints in the Z-direction, at the free edge of the overhanging part of the flange to prevent the development of

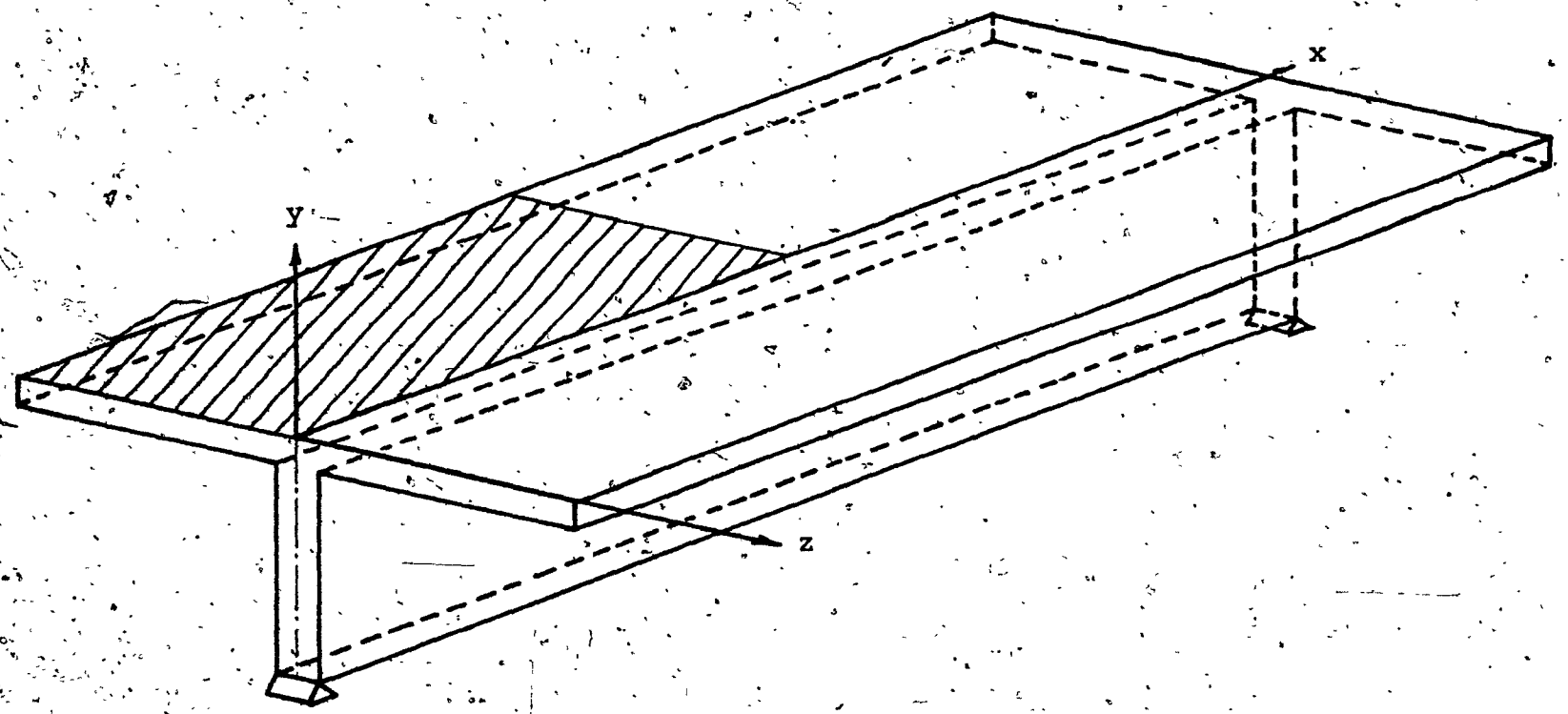

FIG. 3.3 Simply Supported T-Beam

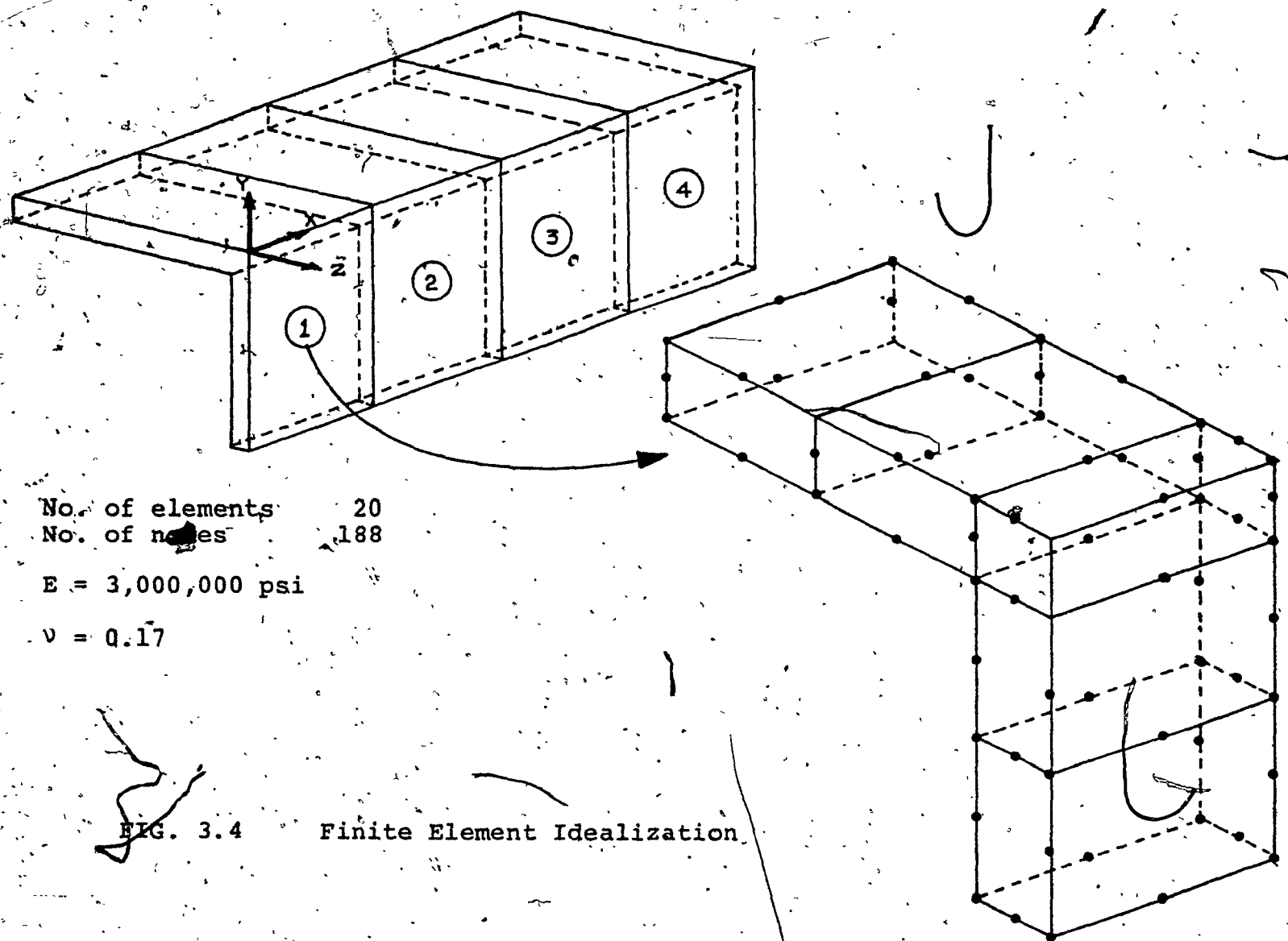

No. of elements 20
No. of nodes 188

E = 3,000,000 psi

ν = 0.17

FIG. 3.4 Finite Element Idealization

antielastic curvature. Flange stresses at the mid-span of the beams are presented in Table 3.2.

3.9 ANALYSIS OF CONTINUOUS BEAM

The two-span continuous beam chosen for finite element analysis has the same cross-sectional properties as that of Beam 2, in Fig. 2.6. Fig. 3.5 shows the dimensions of the test beam. A uniformly distributed load of 1000 lbs per linear ft is applied on both the spans. Due to symmetry, only the hatched area ABCD need be analyzed. Fig. 3.6 indicates the discretization scheme. Proper boundary conditions are prescribed to simulate the continuous support.

The stresses at the top and bottom surfaces of the flange plate are tabulated in Tables 3.3 and 3.4.

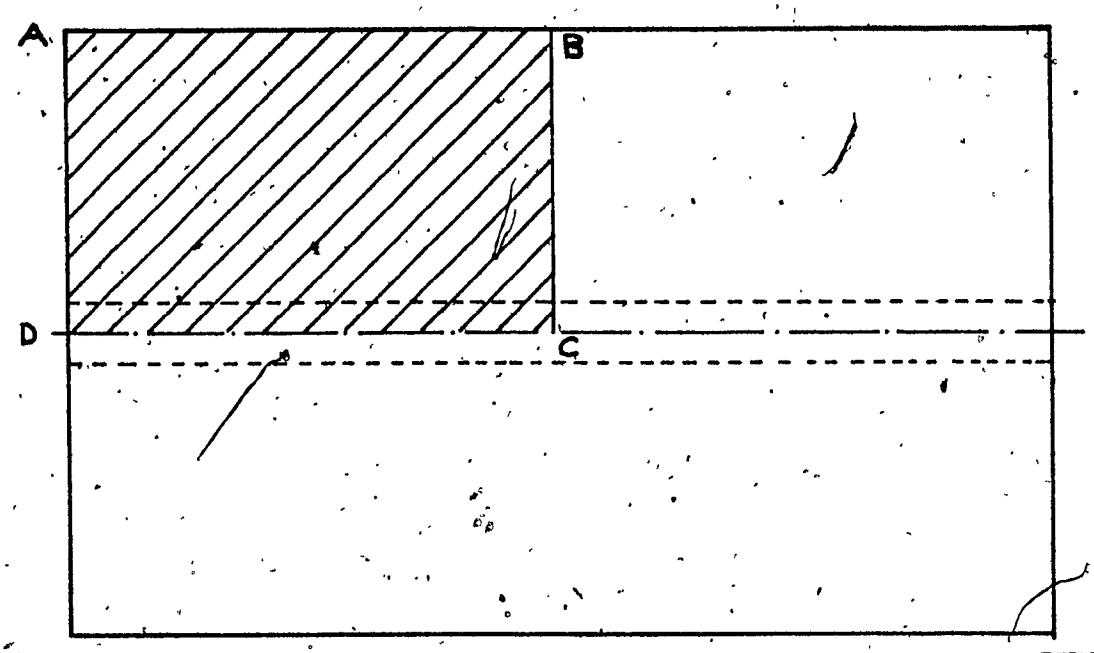

(a)

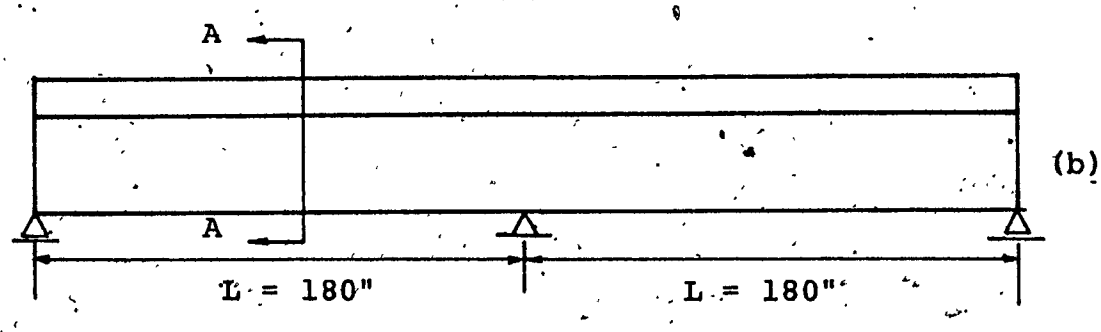

(b)

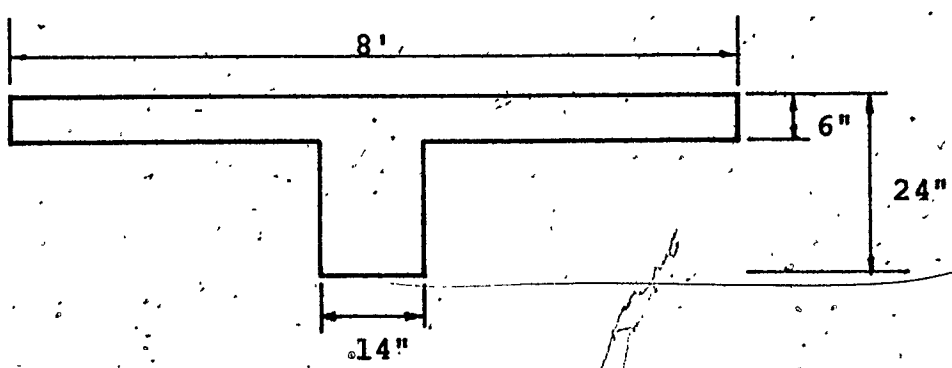

(c) Section A-A

FIG. 3.5 Two Span Test Beam

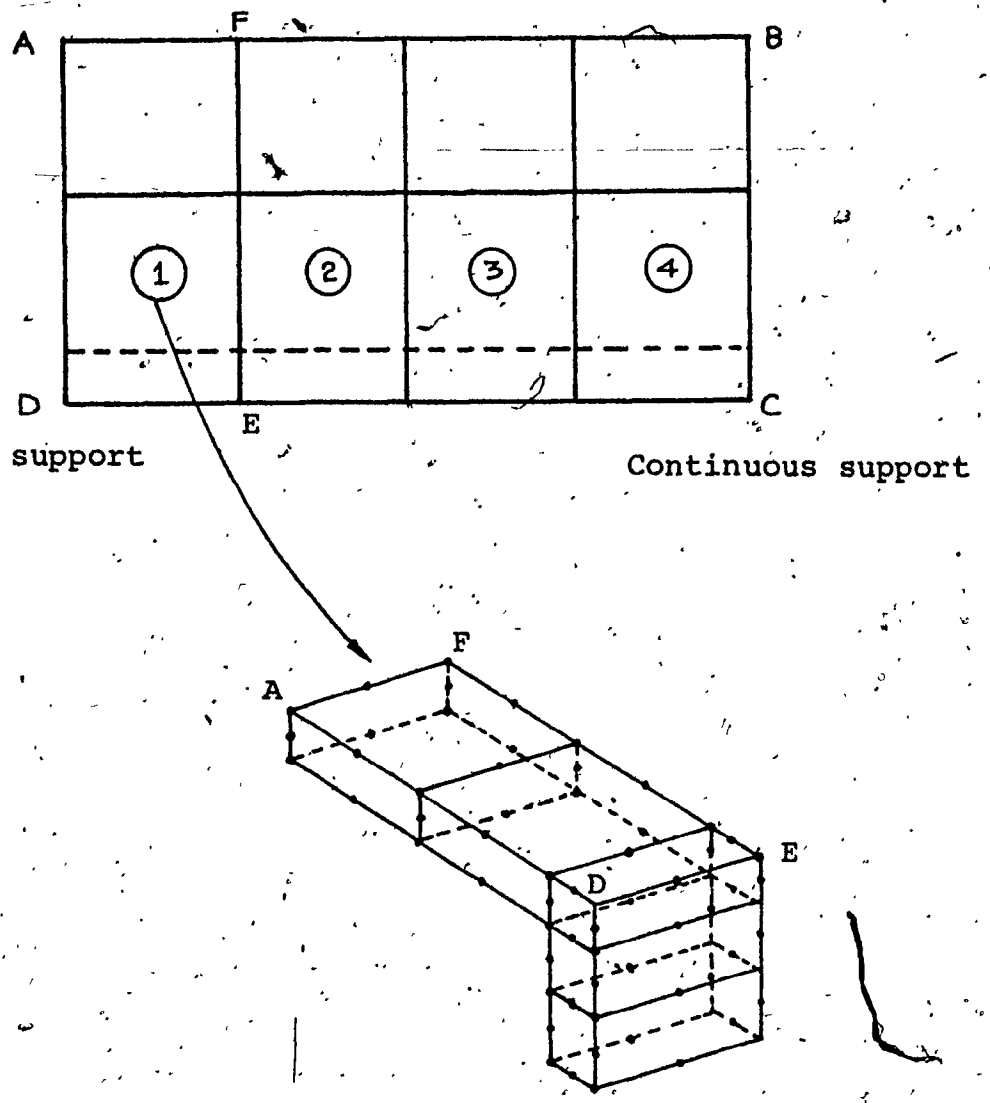

FIG. 3.6 Idealization Scheme

FIG. 3.6

TABLE 3.2

Longitudinal Stresses σ_x in the Flange Plate at midspan: Finite Element Method

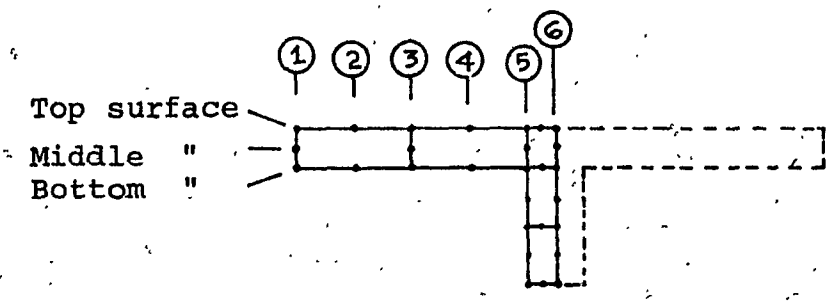

		Location					
		1	2	3	4	5	6
BEAM 1	Top	-28.3	-31.1	-41.1	-55.9	-72.6	-74.7
	Mid.	- 3.6	-	-12.4	-	-39.7	-42.5
	Bot.	+21.1	+20.0	+16.5	+ 9.4	- 7.1	-11.9
BEAM 2	Top	-62.7	-63.7	-67.0	-72.9	-79.7	-82.1
	Mid.	-28.2	-	-32.6	-	-45.2	-47.8
	Bot.	+ 6.2	+ 5.3	+ 2.0	- 2.5	-11.3	-15.1
BEAM 3	Top	-107.3	-107.5	-108.5	-110.5	-112.8	-114.7
	Mid.	- 66.7	-	- 63.2	-	- 72.2	- 74.2
	BOT.	-26.3	-26.5	-27.6	-28.9	- 32.3	- 35.2

NOTE: Stresses are in psi
"-" compression
"+" tension

TABLE 3.3

Top Surface Stresses for Two-Span Beam:
Finite Element Method

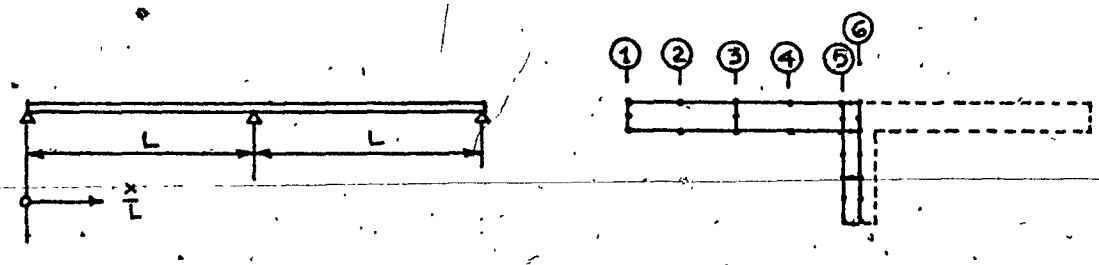

$\frac{x}{L}$	Location					
	①	②	③	④	⑤	⑥
0.125	-14.3	-	-17.9	-	-27.3	-29.4
.25	-25.9	-27.4	-31.1	-38.8	-47.5	-50.6
.375	-32.9	-	-37.1	-	-49.7	-51.9
.50	-29.6	-30.6	-34.0	-38.8	-45.1	-47.5
.625	-18.7	-	-21.2	-	-31.4	-33.9
.75	+ 6.0	+ 5.0	+ 4.9	- 1.6	- 8.4	-10.9
.875	+26.4	-	+30.6	-	+45.8	+47.8
1.0	+29.1	+33.3	+39.8	+62.8	+86.5	+92.8

NOTE: Stresses are in psi
"-" compression
"+" tension

TABLE 3.4

Bottom Surface Stresses for Two-Span Beam:
Finite Element Method

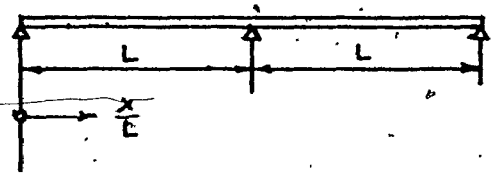

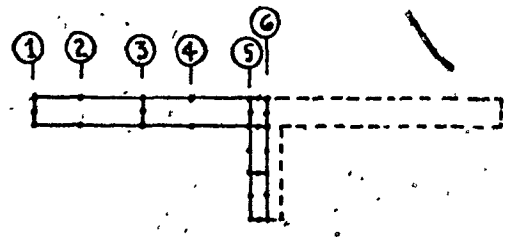

$\frac{x}{L}$	Location					
	1	2	3	4	5	6
0.125	+ 4.9	–	+ 2.9	–	- 5.5	- 7.6
.25	+ 6.0	+ 4.9	+ 1.4	- 2.3	-10.0	-13.4
.375	+ 9.1	–	+ 6.1	–	- 7.5	-11.8
.50	+ 6.2	+ 5.0	+ 2.2	- 0.6	- 9.1	-11.5
.625	+ 8.1	–	+ 5.8	–	- 4.7	- 8.5
.75	- 1.7	- 0.8	- 0.6	- 0.7	- 0.9	- 5.5
.875	-12.4	–	- 9.0	–	+ 7.8	+13.1
1.0	- 9.0	- 8.2	- 5.0	+ 3.0	+13.6	+25.3

NOTE: Stresses are in psi
"–" compression
"+" tension

CHAPTER 4

DISCUSSION OF RESULTS

CHAPTER 4

DISCUSSION OF RESULTS

Stresses in the flange of T-beams have been studied by the classical method and by the finite element technique using 20-node isoparametric solid elements. Longitudinal stresses σ_x at the midspan of the beams shown in Tables 2.1 and 3.2, are plotted in Figs. 4.1, 4.2 and 4.3, to provide a comparative basis. Stress variations at the top, middle and bottom surfaces of the flange plate are compared.

It is seen that near the rib, stresses obtained from both methods are in good agreement. However, for wide flanges, away from the rib, there is a marked difference, particularly for the top and bottom surfaces. This is attributed to the fact that the classical method assumes only the in-plane actions of the flange plate, while in the finite element treatment, bending of the plate is also taken into account.

The depth of the flange plate in the examples is 6 inches, which is not quite as thin as that required by the classical method. For wide flanges with such thicknesses, three-dimensional analysis does show tension at the bottom face of the plate, as can be seen in Figs. 4.1 and 4.2. The average stress at any point along the flange across its thickness can be obtained from the stresses at the middle

surface, which for both methods are clearly shown to be in close agreement. For Example 1, the finite element results are presented as a stress block in Fig. 4.4.

Effective widths for the three beams are listed in Table 4.1. Calculation of b_e by the classical method has been described in Chapter 2. In the case of finite element analysis, the total compression on the overhang is first obtained from the volume of the stress block computed by numerical integration. This compressive force is then divided by the product of the flange thickness and the maximum stress at the middle surface of the flange plate, yielding the effective width of the overhanging portion of the flange. A third set of values has been computed from the requirements of the Canadian Code for the Design of Reinforced Concrete Structures CSA Standard A23.3 - 1970.

For Beam 1, which has the widest flange, the classical approach gives a slightly higher value of the effective width. For the other cases, the agreement is excellent. The effective width of a T-beam is also dependent upon the type of loading. The Code, however, does not make any distinction in this regard. Considering the wide range of variables that has to be covered by the Code, it is evident that the Code values of b_e are within the range of practical design purposes.

Rib stresses at the midspan, tabulated in Table 4.2,

also reflect the observations made above. The stresses at the bottom of the rib are in excellent agreement.

Compressive forces on the flange are presented in Table 4.3. Table 4.4 provides a comparative guide to the midspan deflections. It is noted that the finite element analysis also includes the deflection due to shear. In the other two approaches, the deflections are computed, assuming that the effective width b_e at the midspan is constant throughout the length of the beam, which is not strictly true. Effective widths vary along the length of the beam. The values obtained, however, are within the acceptable range.

For the continuous beam, the finite element analysis has provided a clear picture of the distribution of longitudinal stresses across the width of the flange. Stresses at the top surface of the flange have been plotted in Fig. 4.5. Stress patterns for the section over the continuous support are shown in Fig. 4.6. Effective widths b_e at various sections are also listed in Table 4.5. These are compared with the value obtained from the Code. Variation of the ratio b_e/b along the length of the beam is shown in Fig. 4.7.

At the point of contraflexure, where the bending stresses are zero, the usual concept of effective width as defined in Eq. (2.12) loses its significance and does not serve any practical purpose. Hence, in the neighbourhood of this point, the curve is left undefined. Since in reinforced

concrete design tension is taken by the steel reinforcement, the question of effective flange width over the support does not arise. However, for steel plate construction this information is useful.

Table 4.6 shows that the maximum stresses in the flange obtained by using the Code are about 20% larger than those given by the finite element analysis. Thus, for this particular test case, the effective width computed on the basis of the Code, provides a larger margin in the maximum stresses. It is recognized, however, that the Code has to make provision for a safe margin for a wide variety of loading cases.

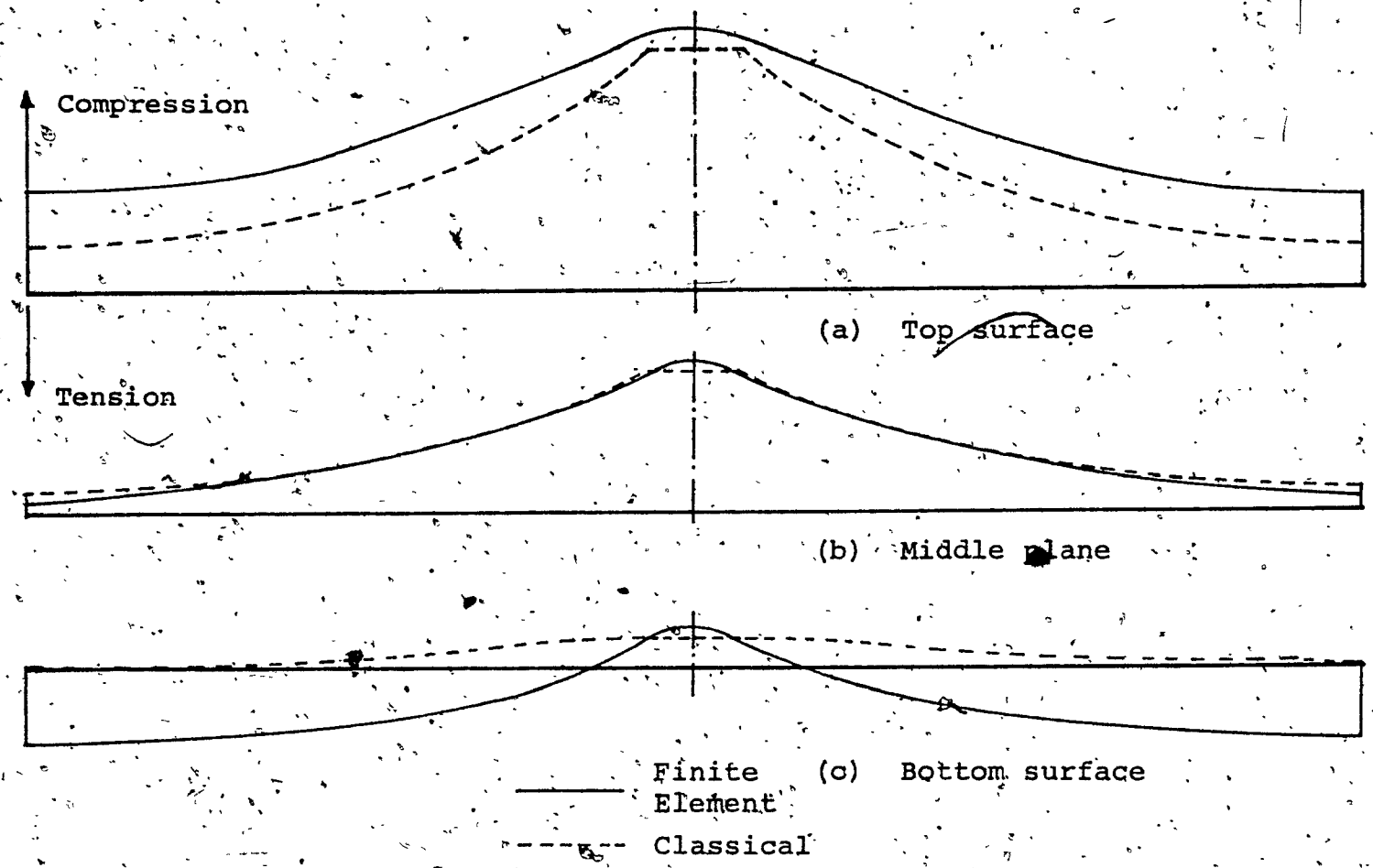

FIG. 4.1 Longitudinal Stresses σ_x in the Flange at Midspan: Beam 1

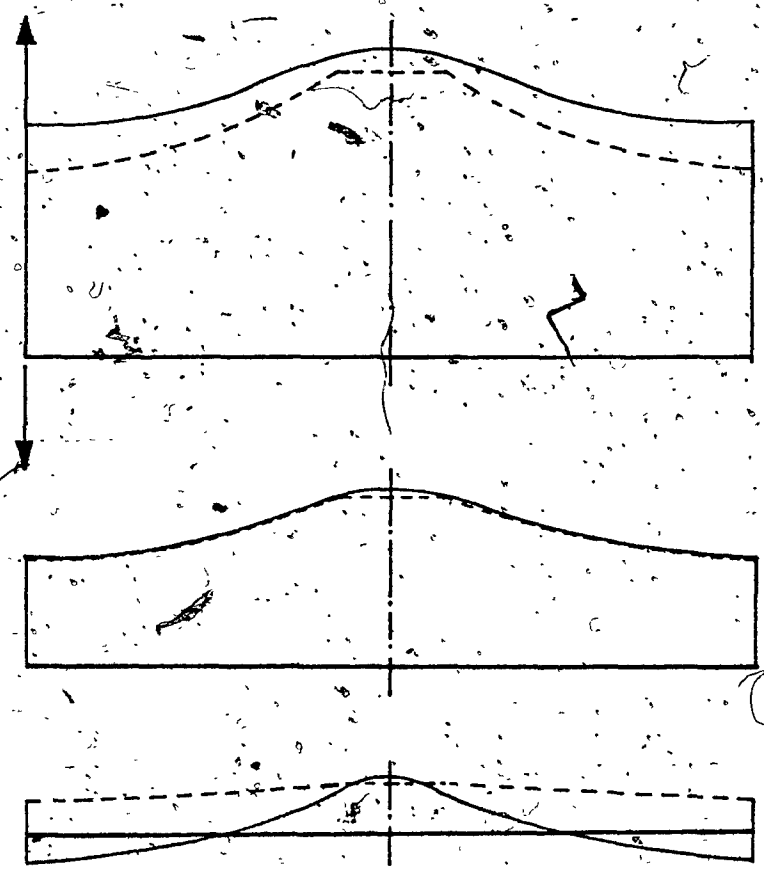

—— Finite element

---- Classical

FIG. 4.2 Longitudinal Stresses σ_x in the Flange at Midspan: Beam 2

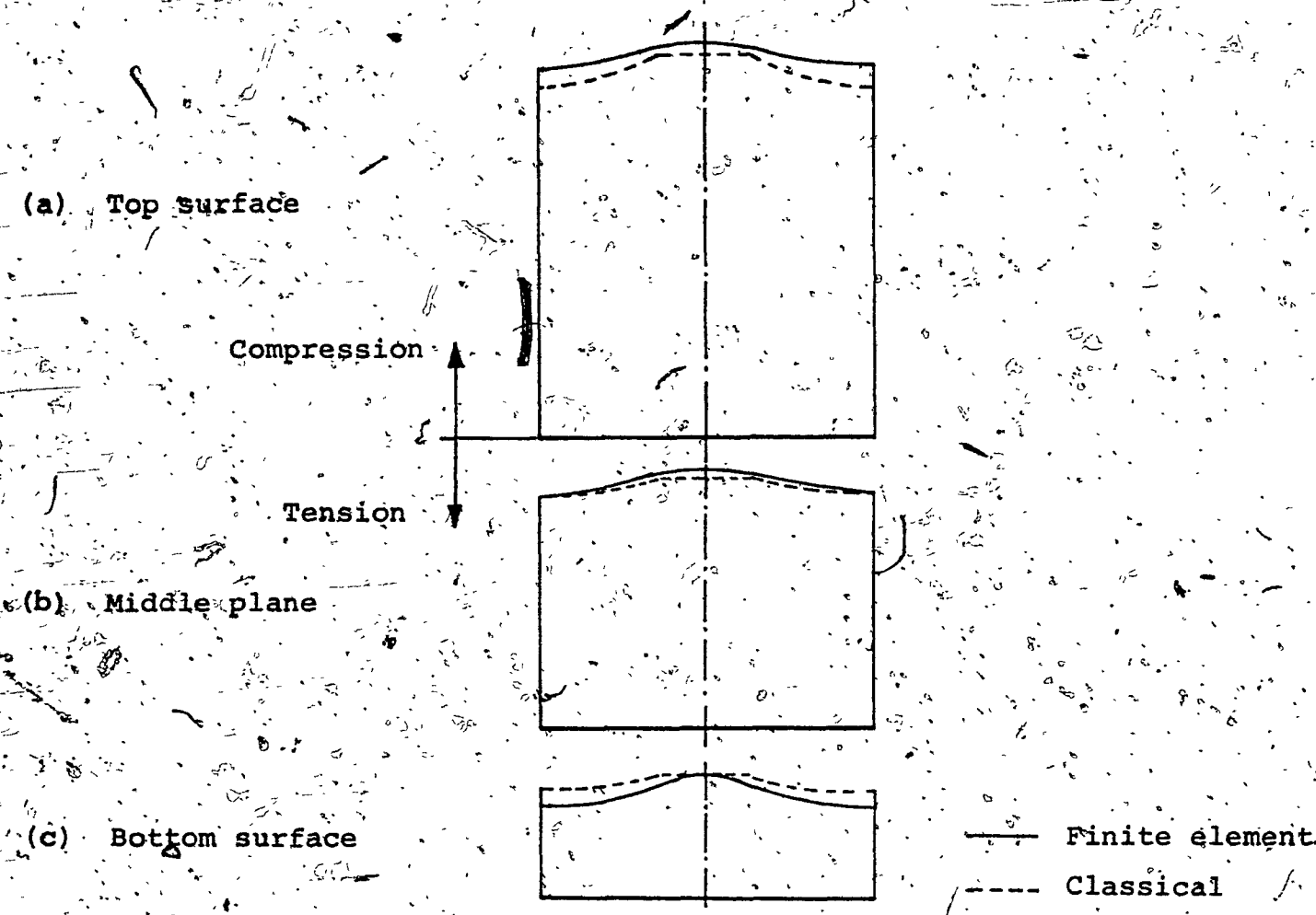

FIG. 4.3 Longitudinal Stresses σ_x in the Flange at Midspan: Beam 3

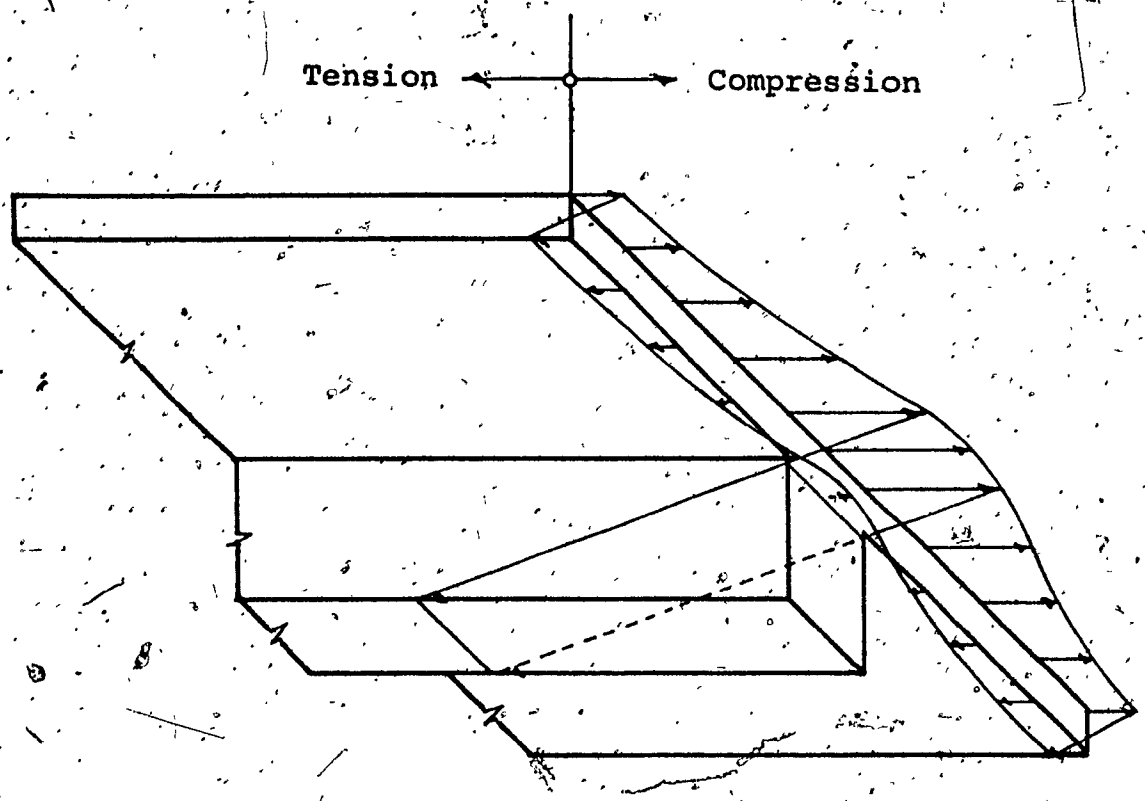

FIG. 4.4 Stress Block at Midspan of Beam 1: Finite Element Method

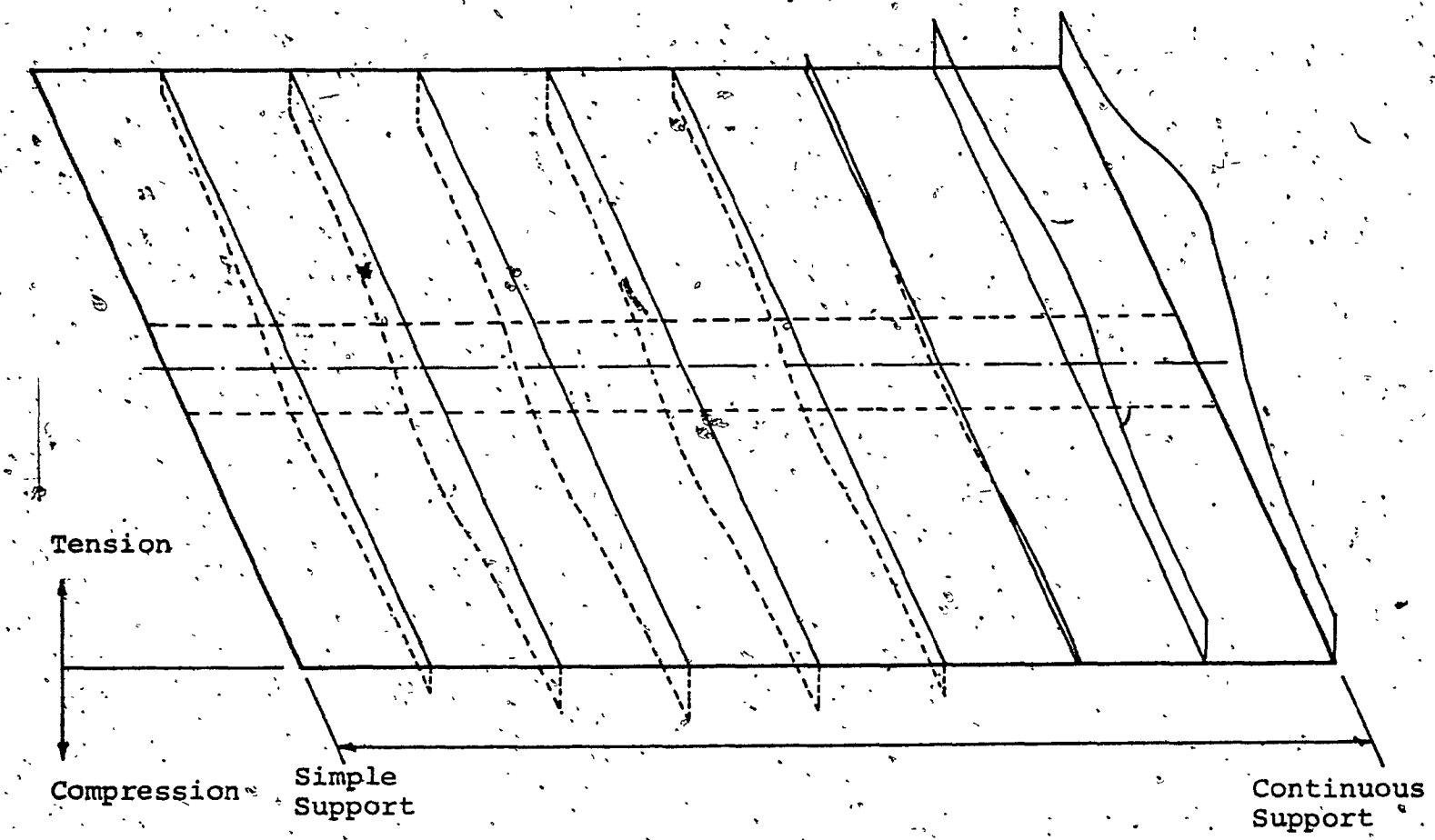

FIG. 4.5 Top Surface Stresses: Two Span Beam

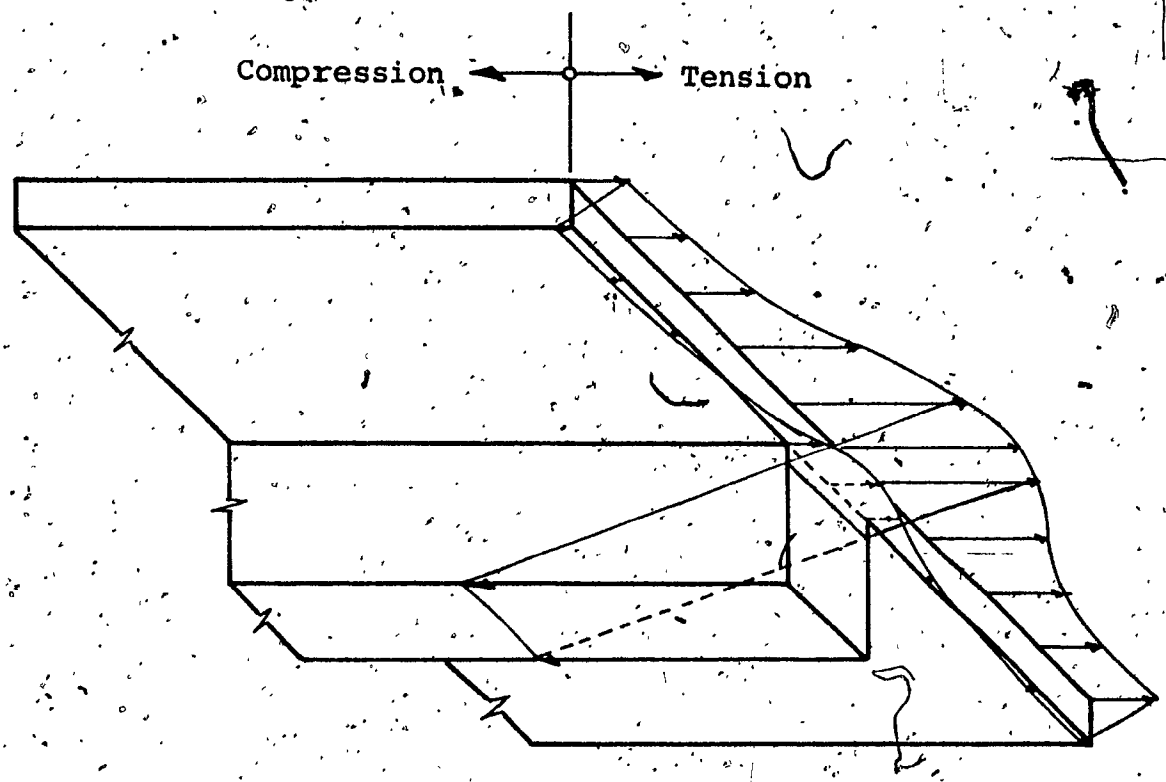

FIG. 4.6 Stress Distribution Over the Mid-Support: Two-Span Beam

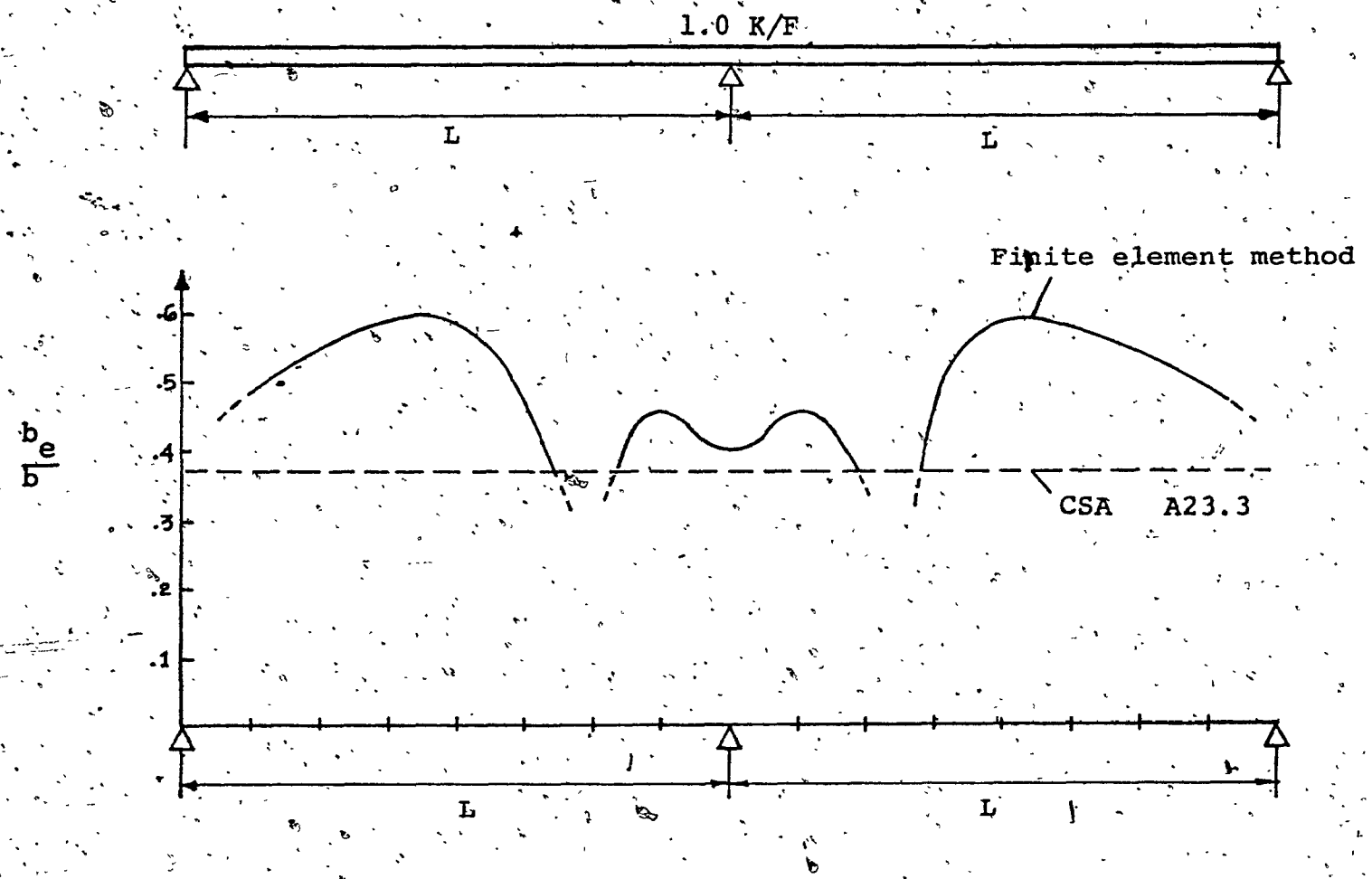

FIG. 4.7 Variation of Ratio b_e/b for the Two-Span Beam

TABLE 4.1

Comparison of Effective Widths b_e at Midspan

	BEAM 1	BEAM 2	BEAM 3
Classical	38.49 in	31.30 in	16.15 in
F. E. M.	32.92 in	29.22 in	15.71 in
CSA A23.3	29.00 in	29.00 in	17.00 in

TABLE 4.2

Midspan Stresses σ_x at Centre Line of Rib

	BEAM 1		BEAM 2		BEAM 3	
	Top	Bot.	Top	Bot.	Top	Bot.
Classical	- 68.9	+174.7	- 77.4	+178.8	-110.2	+193.6
F.E.M.	- 74.7	+170.6	- 82.1	+179.8	-114.6	+195.8
CSA A23.3	- 80.7	+180.3	- 80.7	+180.4	-107.4	+192.4

NOTE: Stresses are in psi
"-" compression
"+" tension

TABLE 4.3

Comparison of Compression on Flange at Midspan

	Compressive force per unit flange thickness (lbs/in)	
	Classical	F.E.M.
BEAM 1	1480.9	1399.0
BEAM 2	1420.2	1395.9
BEAM 3	1166.8	1166.3

TABLE 4.4

Comparison of Midspan Deflections

	Midspan Deflection (inch)		
	F.E.M. *	Classical **	CSA 23.3 **
BEAM 1	0.012816	0.011937	0.012218
BEAM 2	0.013511	0.012491	0.012218
BEAM 3	0.015516	0.014509	0.014025

* Top surface deflection
** Computed midspan b_e assumed constant throughout.

TABLE 4.5

Effective Widths for the Continuous Beam

$\frac{x}{L}$	F.E.M.		C.S.A. Standard A23.3	
	b_e(in)	b_e/b	b_e(in)	b_e/b
0.125	20.00	0.487	15.5	0.378
.250	21.96	0.536		
.375	23.01	0.562		
.500	24.21	0.590		
.625	18.73	0.457		
.750				
.875	18.64	0.455		
1.000	16.39	0.400		

TABLE 4.6

Maximum Stresses in the Continuous Beam

		F.E.M.	CSA A23.3
Flange	Max. Compression	-51.9	-63.3
	Max. Tension	+92.8	+112.5
Bottom of Rib	Max. Compression	-176.6	-194.0
	Max. Tension	+99.8	+109.0

CHAPTER 5

CONCLUSIONS

CHAPTER 5

CONCLUSIONS

A computer program has been developed for the three-dimensional finite element analysis of T-beams using the 20-node isoparametric hexahedron element. The classical method, taking into account only the membrane action of the flange of the T-beams has also been outlined.

Both methods were used to analyze a number of simply supported beams. A two-span continuous beam was also analyzed by the finite element technique.

The effective flange width and the distribution of longitudinal stresses in the flange were investigated. The results were compared with those obtained by using the requirements of CSA Standard A23.3, 1970.

Based on this study, the following conclusions are drawn.

(1) T-beams with wide and relatively thick flanges can be readily investigated by finite element method using the three-dimensional elements. It permits a closer study of the bending effect of the flange.

(2) For simply supported T-beams with a moderate flange thickness, the classical treatment provides a satisfactory measure of the stresses, even though

only the membrane action of the flange plate is accounted for.

(3) The values of effective width given by CSA Standard A23.3/1970, provide stresses within the acceptable limits of practical design.

REFERENCES

REFERENCES

[1] Von Karman, Th., Die Mittragende Breite, August-Föppl-Festschrift, 1924, pp.114-127.

[2] Chwalla, E., Die Formeln zur Berechnung der voll Mittragenden Breite Dünner Gurt - und Rippenplatten, Der Stahlbau, 1936, p.73.

[3] Koepcke, W., and Denecke, G., Die Mitwirkende Breite der Gurte von Plattenbalken, Deutscher Ausschuss für Stahlbeton, Heft 192, Verlag Wilhelm Ernst & Sohn, Berlin, 1967.

[4] Marguerre, K., Über die Beanspruchung von Plattenträgern, Der Stahlbau, 1952, pp. 129-132.

[5] Brendel, G., Strength of the Compression Slab of T-Beams Subject to Simple Bending, Journal of the American Concrete Institute, Vol. 61, 1964.

[6] Dischinger, F., Taschenbuch für Bauingenieure, Vol.1, Springer Verlag, Berlin, 1955, pp.842-847.

[7] Girkmann, K., Flächentragwerke, Springer Verlag, Wien, 1963.

[8] Timoshenko, S., and Goodier, J.N., Theory of Elasticity, McGraw-Hill Book Co., 1951.

[9] Beton-Kalender 1972, Vol. 1, Verlag Wilhelm Ernst & Sohn, Berlin, 1972, pp.631-634.

[10] Abdel-Sayed, G., Effective Width of Steel Deck-Plate in Bridges, Proceedings of the American Society of Civil Engineers, Vol. 95, No. ST7, July, 1969.

[11] Przemieniecki, J.S., Theory of Matrix Structural Analysis, McGraw-Hill, N.Y., 1968.

[12] Zienkiewicz, O.C., The Finite Element Method in Engineering Science, McGraw-Hill, 1971.

[13] Desai, C.S., and Abel, J.F., Introduction to the Finite Element Method, Van Nostrand Reinhold Co., 1972.

[14] Holand, I., and Bell, K., Ed., Finite Element Methods in Stress Analysis, Tapir, Trondheim, Norway, 1969.

[15] Tottenham, H. and Brebbia, C., Editors, Finite Element Techniques in Structural Mechanics, Lectures presented at Southampton University in April, 1970. Stress Analysis Publishers, Southampton, England.

[16] Proceedings of the Symposium on Applications of Finite Element Methods in Civil Engineering, Vanderbilt University, Nashville, Tenn., 1969.

[17] Proceedings of the Speciality Conference on Finite Element Methods in Civil Engineering, McGill University, Montreal, Canada, 1972.

[18] Ergatoudis, J.G., Irons, B.M. and Zienkiewicz, O.C., Three-Dimensional Stress Analysis of Arch Dams and Their Foundations, Proceedings of Symposium on Arch Dams, Institution of Civil Engineers, London, 1968.

[19] Ergatoudis, J.G., Irons, B.M. and Zienkiewicz, O.C., Curved Isoparametric Quadrilateral Elements for Finite Element Analysis, International Journal of Solids and Structures, Vol. 4, No. 1, Jan. 1968.

[20] Luft, Rene W., Roesset, Jose M., Connor, Jerome J., Automatic Generation of Finite Element Matrices, Journal of the Structural Division, ASCE, Vol. 97, No. ST1, Jan. 1971.

[21] Melosh, R.J., and Bamford, R.M., Efficient Solution of Load-Deflection Equations, Journal of the Structural Division, ASCE, Vol. 95, No. ST 4, Apr. 1969, pp.661-676.

[22] Irons, B.M., A Frontal Solution Program for Finite Element Analysis, International Journal for Numerical Methods in Engineering, Vol. 2, No. 1, Jan. 1970, pp.5-32.